Palaeogeography, Palaeoclimatology, Palaeoecology 613 (2023) 111424

Contents lists available at ScienceDirect

Palaeogeography, Palaeoclimatology, Palaeoecology

journal homepage: www.elsevier.com/locate/palaeo

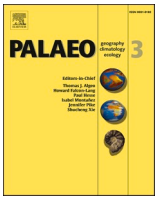

New constraints on the closure of the Betic Seaway and the western Mediterranean palaeoclimate during the Messinian Salinity Crisis from the Campo Coy Basin (SE Spain)

Victoriano Pineda [a,*], David Artiaga [b], Francisco J. Ruiz-Sánchez [c], Plini Montoya [c], Jesús M. Soria [d], Hugo Corbí [d], Luis Gibert [a]

[a] Dpt. de Mineralogia, Petrologia i Geologia Aplicada., Universitat de Barcelona, 08028 Barcelona, Spain
[b] CCiTUB Scientific and Technological Centers, Universitat de Barcelona, 08028 Barcelona, Spain
[c] Dpt. de Botànica i Geologia, Universitat de València, 46100 Burjassot, Spain
[d] Dpto. de Ciencias de la Tierra y Medio Ambiente, Universidad de Alicante, 03080 Alicante, Spain

ARTICLE INFO

Editor: L Angiolini

Keywords:
Betic Neogene Basins
Betic Seaway
Zanclean
Evaporites
Tortonian

ABSTRACT

The Campo Coy Basin (SE Spain) exposes >1 km of sedimentary succession with a variety of rocks including a thick evaporitic succession previously associated with the Messinian time. These evaporites were supposedly deposited in a restricted Mediterranean-Atlantic seaway connecting the Lorca and Guadix-Baza basins, although no chronological or geochemical data existed. Here we use palaeomagnetism together with vertebrate and foraminifera biostratigraphy to constrain the age of the Campo Coy succession between <9 Ma and 4.7 Ma. We use geochemistry ($\delta^{34}S$, $\delta^{18}O$ and $^{87}Sr/^{86}Sr$ values) of the gypsum deposits to evaluate their marine or continental origin. In addition, we describe the underlying and overlying lithostratigraphic units to reconstruct the palaeogeographic evolution of this region. Our results show that the sediments were deposited in a continental environment, indicating that the Betic Seaway was already closed in this region during the late Tortonian and that the neighbouring marine basins of Guadix-Baza and Lorca were disconnected during that time. The $\delta^{34}S$, $\delta^{18}O$ and $^{87}Sr/^{86}Sr$ values of the gypsum indicate recycling from the Triassic sulphates. Sedimentary facies of the evaporites point to an environment dominated by a saline lake with continental sabkha episodes developed during the driest periods. Well-defined and laterally continuous evaporitic cyclicity suggests an orbital forcing and high sedimentation rates preceding the Messinian Salinity Crisis (MSC). Alluvial deposits are contemporaneous with the MSC indicating a dry continental environment in this region during the Mediterranean restriction. Overlaying lacustrine carbonates are rich in small vertebrate fauna including African species that migrated to Europe during the MSC. These carbonates have low $\delta^{18}O$ and $\delta^{13}C$ values characteristic for freshwater input in an open lake just after the Zanclean flood, suggesting that a wet climate followed the MSC.

1. Introduction

During the early-middle Tortonian, the Mediterranean Sea and the Atlantic Ocean were connected through the Betic and Rifian seaways, corresponding with the foreland of the Betic and Rif Cordilleras, respectively. Due to the Africa and Eurasia plate convergence, the Betic Seaway (or Betic Strait) emerged locally and transformed into a series of interconnected marine basins. These basins were restricted and isolated during the late Tortonian and the early Messinian (Colom, 1952; Sanz de Galdeano, 1990; Esteban et al., 1996; Soria et al., 1999; Chalouan et al., 2001; Tent-Manclús et al., 2008; Corbí et al., 2012; García-Veigas et al., 2019). The closure of the Betic and Rifian seaways favoured the restriction of the Mediterranean, probably leaving as a unique Atlantic-Mediterranean connection the palaeo-Gibraltar strait (Krijgsman et al., 2018). This new situation favoured the onset of the so-called Messinian Salinity Crisis (MSC), forming the youngest saline giant on Earth which accumulated 5% of the global ocean's salt in the Mediterranean basin (Ryan, 1973; Haq et al., 2020) between 5.97 and 5.33 Ma (Krijgsman et al., 1999; Van Couvering et al., 2000; Rouchy and Carusso, 2006; Manzi et al., 2013). During the restriction of the Betic Seaway, numerous

* Corresponding author.
E-mail address: vpinedagon@ub.edu (V. Pineda).

https://doi.org/10.1016/j.palaeo.2023.111424
Received 13 May 2022; Received in revised form 7 January 2023; Accepted 18 January 2023
Available online 20 January 2023

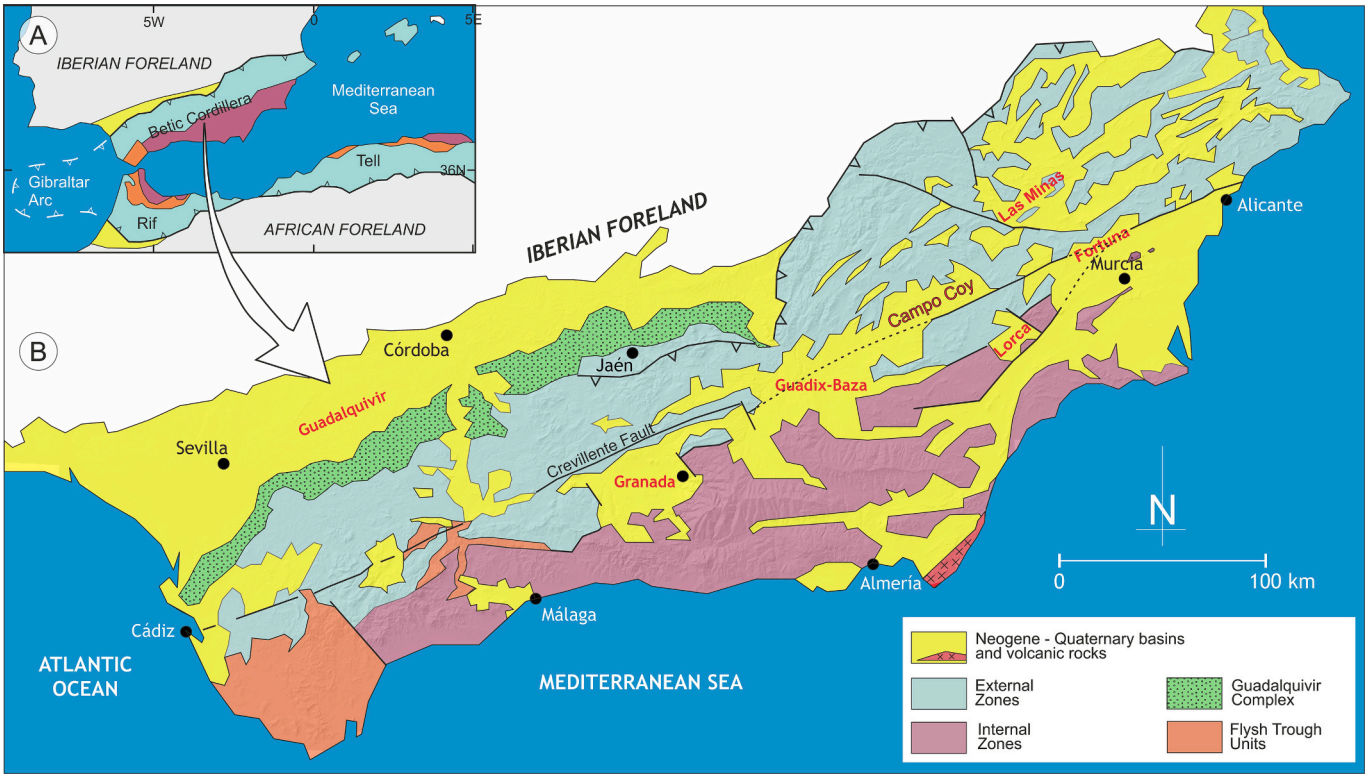

Fig. 1. A) Situation of the Gibraltar Arc and the Betic and Rif Cordilleras (Modified from Crespo-Blanc et al., 2016) B) General geological map of the Betic Cordillera, with the location of the Campo Coy Basin and other Neogene inner basins (Modified from Soria et al., 1999 and Corbí et al., 2012).

evaporite deposits were formed in the associated Betic basins. Depending on their position with respect to the Mediterranean Sea, these basins are divided into "marginal basins" and "inner basins". The marginal basins (Sorbas, Níjar, Bajo Segura, among others), were connected to the Mediterranean Sea during the Messinian and accumulated evaporite deposits assigned to the MSC (e.g., Rouchy, 1982; Krijgsman et al., 2001; Rouchy and Carusso, 2006; Soria et al., 2008; Roveri et al., 2009; Corbí et al., 2016). The inner basins, such as Granada, Lorca, Fortuna, Las Minas and Jumilla were located more inland, and their evaporite formations developed before the MSC in a transitional (from marine to continental) or continental environment (Pineda et al., 2021 and references therein). Descriptions of continental successions contemporaneous to the MSC are uncommon in the Mediterranean region, with only one studied example in central Anatolia (Meijers et al., 2018). The continental vertebrate fossil content of the MSC is included in the faunal zone MN13, assigned to the Ventian mammal age (Aguirre et al., 1976) which covers the period of 7 to 5 Ma (Morales et al., 2013). This faunal zone includes different faunal exchanges between Africa and Europe (Gibert et al., 2013 and references therein).

The Campo Coy basin, located between the Lorca and Guadix-Baza basins, belongs to the group of the inner Betic basins (Fig. 1). Previous works proposed that, during the late Tortonian-Messinian, the Campo Coy basin was part of the Betic Seaway, connecting the Guadix-Baza basin to the southwest and the Lorca Basin to the southeast (Soria et al., 1999; Corbí et al., 2012) and a Messinian age was assigned to the Campo Coy evaporites (Soria et al., 1999). In contrast with other Betic basins, only preliminary information about the Campo Coy Basin is available in some studies focused on palaeontology (De Bruijn et al., 1975; Freudenthal et al., 1998), evaporites (Salvany and Ortí, 1990; Artiaga et al., 2020) and geological mapping (Baena, 1974; Paquet et al., 1974). Nonetheless, the Campo Coy Basin deserves further attention since it constitutes a key area for reconstructing the closure of the Betic Seaway and the continental history of the Messinian Salinity Crisis in the western Mediterranean. Here we present a multidisciplinary study, which for the first time constrains the age of the Campo Coy deposits. A new description and illustration of the lithostratigraphy, together with a petrological characterization of the gypsum deposits, isotope analyses and palaeontological data allow us to interpret the latest Neogene palaeogeographic evolution of this region.

2. Geological setting

The Betic Cordillera (SE Spain), together with the Rif Cordillera (N Morocco), form an arcuate orogen known as Gibraltar Arc (Crespo-Blanc et al., 2016 and references therein), which surrounds the Alboran Sea and is limited to the north and south by the foreland massifs of the Iberia and Africa plates (Fig. 1A). The Betic Cordillera consists of three main geological domains: Internal Zones, External Zones and Neogene-Quaternary Basins (Fig. 1B). The Internal Zones constitute an allochthonous lithospheric block of metamorphic rocks (Alborán Block, Andrieux et al., 1971) derived from the Mesomediterranean Microplate, which migrated westwards until colliding with Iberia and Africa plates (Durand Delga and Fontboté, 1980; Guerrera and Martín-Martín, 2014). The External Zones are formed by sedimentary rocks and represent the Mesozoic and Cenozoic sedimentary cover of the South-Iberia margin (Lonergan and White, 1997). The External Zones are divided into two palaeogeographic subdomains: the shallower Prebetic and the deeper Subbetic. Both the Internal and External zones constitute the basement of the post-orogenic Neogene-Quaternary basins.

The Campo Coy Basin is a Neogene basin located in the eastern part of the Betic Cordillera, in the western Murcia province (Spain). This basin has a SW-NE 22 km-long major axis and a surface area of 150 km^2, with a sedimentary record onlapping the Subbetic basement (Fig. 2A). The southern margin is limited by the Crevillente Fault and evaporitic Triassic materials with abundant igneous ophite blocks. These Triassic materials have been interpreted as extruding along the longitudinal axis of a flower structure, marked by the Crevillente fault, in a transpressive tectonic context (De Smet, 1984). To the east, west and north the basin is

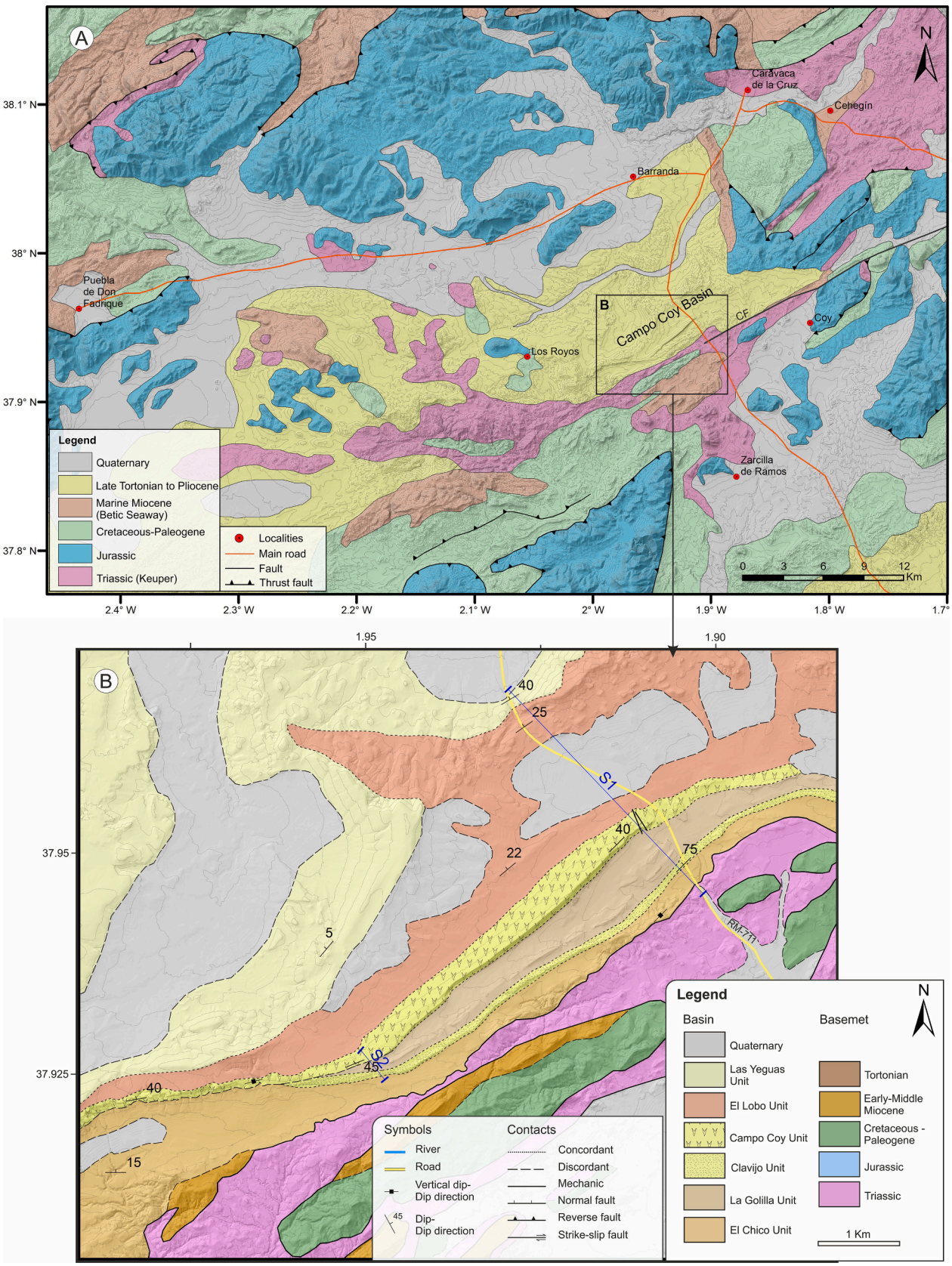

Fig. 2. A) Regional Geological map of the Lorca-Caravaca area. CF: Crevillente Fault. B) Geological map of the studied area in the Campo Coy Basin, with the location of the studied stratigraphic sections (Modified from Baena, 1974 and Artiaga et al., 2020). 'Mechanic' refers to the contact between the Triassic diapir and the sedimentary cover.

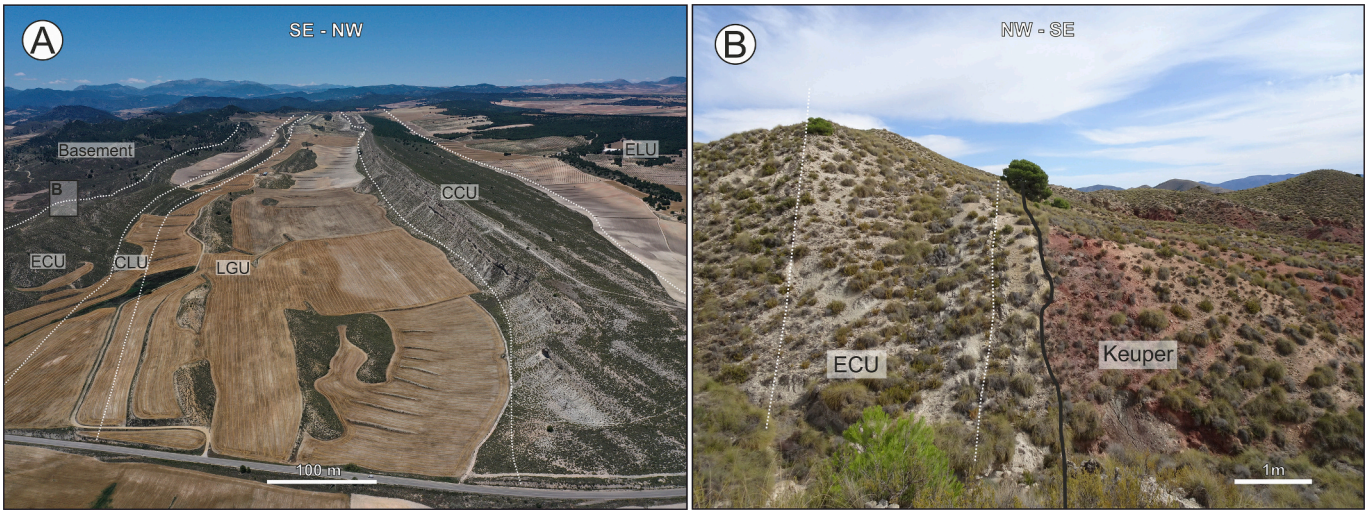

Fig. 3. A) Aerial photo of the Campo Coy Basin taken in a SW direction from the RM-711 road, and distinction of the observed units. ECU: El Chico Unit; CLU: Clavijo Unit; LGU: La Golilla Unit; CCU: Campo Coy Unit; ELU: El Lobo Unit. B) Contact between the Triassic basement (Keuper facies) and the El Chico Unit (ECU). Note the vertical bedding in the ECU.

limited by Jurassic and Cretaceous reliefs (Fig. 2A). The most recent materials of the basement are Late Miocene marine coastal deposits that crop out to the southeast and northeast of the basin (Baena, 1974; Paquet et al., 1974).

The deposits of the Campo Coy Basin are dominantly dipping in an NNW direction, with the dip increasing considerably along the contact with the Triassic basement to the south (Fig. 2B, 3). The sedimentary infill (>1000 m) of the Campo Coy basin consists of six lithostratigraphic units which are indicated here with local names: El Chico, Clavijo, La Golilla, Campo Coy, El Lobo and Las Yeguas units (Figs. 3, 4).

3. Materials and methods

3.1. Petrology

Thin sections of gypsum and carbonate samples ($n = 20$) have been studied petrographically using a Zeiss Axiophot microscope. All types of gypsum lithofacies from the Clavijo and Campo Coy units (Fig. 4) were sampled. Detailed observations of the crystal habits and textural characteristics of gypsum and carbonates were performed using a Jeol-7100 Field Emission SEM equipped with an energy dispersive X-Ray detector for element analysis (EDX) at the Scientific and Technological Centers of the University of Barcelona (CCiTUB).

3.2. Geochemistry

Sulphur isotope compositions ($\delta^{34}S_{CDT}$) were determined in 31 gypsum samples from Clavijo and Campo Coy units, while oxygen isotope compositions ($\delta^{18}O_{SMOW}$) were measured in 11 of these samples. Measurements were done at the Scientific and Technological Centers of the University of Barcelona (CCiTUB). Samples were dissolved in heated (50 °C) ultrapure water, filtered to eliminate insoluble material and acidified to pH 3 to eliminate carbonates. Dissolved sulfate was reprecipitated as $BaSO_4$ by the addition of a $BaCl_2$ solution. Isotope determinations were performed with an ISOGAS Sira-9 Spectrometer and a Thermo Finigan Delta Plus XP Spectrometer. The analytical error (2σ) is ±0.3‰ for $\delta^{34}S$ and $\delta^{18}O$. Values obtained for the international standard NBS-127 are $\delta^{34}S$: 20.3 ± 0.1‰ and $\delta^{18}O$: 9.3 ± 0.2‰. Gypsum samples ($n = 5$) were analyzed for their $^{87}Sr/^{86}Sr$ ratios at CSIRO (North Ryde, Australia). About 25 mg of each sample were dissolved in 2 ml of >18.2 $M\Omega cm^{-1}$ water overnight and then centrifuged. The supernatant was removed, redissolved in HNO_3 and loaded onto Sr-Spec resin-conditioned columns. The eluted strontium was then loaded onto a Ta filament with H_2O and H_3PO_4 for TIMS (Thermal Ionization Mass Spectrometry) analysis. Isotopic ratios were measured on a VG 354 TIMS with a long-term analytical precision of ±0.000014 measured on NBS-987 ($^{87}Sr/^{86}Sr$:0.710235 ± 0.000014). All the results were normalized to $^{87}Sr/^{86}Sr = 0.1194$.

Stable oxygen and carbon isotopic analyses of carbonate were performed in 7 calcite samples from Las Yeguas Unit. Powdered samples were dissolved in ultrapure water to eliminate soluble sulphates. About 50 μg of the non-soluble fractions (composed of carbonates and minor amounts of detrital silicates) were treated to react in an online Kiel Devicewith 103% H_3PO_4 for 3 and 15 min in vacuum at 70 °C. The obtained CO_2 was analyzed in a Dual Inlet isotope-ratio mass spectrometer (IRMS; Thermo Electron FinniganMAT-252). Values are reported in ‰ with respect to the V-PDB (Vienna-Pee Dee Belemnite) standard, with a precision of ±0.06‰ for $\delta^{18}O$ (VPDB) and ± 0.02‰ for $\delta^{13}C$ (VPDB).

3.3. Palaeomagnetism

The upper 260 m of the S1 section (Fig. 4), which includes the El Lobo and Las Yeguas units, were sampled for palaeomagnetic studies. Palaeomagnetic-oriented samples ($n = 104$) were collected from 52 different strata (2 samples per level) using an electric drill. Only lutites, silts, sands and carbonates were sampled, avoiding coarse-grained lithologies. Samples were collected from fresh outcrops (recent road cuts) or after digging, avoiding weathered materials. Characteristic Remanent Magnetization (ChRM) was determined by stepwise thermal demagnetization at steps of 50 °C below 300 °C, and 40 °C above 300 °C, until the complete demagnetization of the samples at 620 °C. Samples showing a weak magnetization were first demagnetized using alternating fields (A. F.) until 12 mT, and later by thermal demagnetization at 30 °C steps until complete demagnetization. Measures were done on a 2G Enterprises cryogenic magnetometer at the Palaeomagnetism Laboratory of the GEO3BCN-CSIC institute in Barcelona, Spain. Palaeomagnetic directions were calculated by means of principal component analysis (Kirschvink, 1980) using the PALDIR software, developed by the Palaeomagnetic laboratory of Utrecht University. The reliability of the identified ChRM was assessed by applying the fold test (Graham, 1949; Butler, 1992) using the PALDIR software, allowing to discriminate potential false normal directions.

3.4. Palaeontology

Samples of 1 kg of lutites and marls ($n = 35$) from the El Chico and La Golilla units, were collected to study their invertebrate microfossil association. Samples were collected along continuous outcrops covering the entire units. Samples were washed and disintegrated using tap water and sieved with 0.500, 0.125 and 0.063 mm sieves. After sieving, the residue trapped on the sieve was cleaned using ultrasound to remove clay, and later observed under a Zeiss discovery V12 binocular microscope.

Samples of 30–90 kg of dark clays from the Las Yeguas Unit ($n = 8$) were collected and sieved to concentrate micromammal remains. Two key fossiliferous localities, preserving fossil remains of small mammals, have been described in this area: Caravaca (De Bruijn et al., 1975) and Almudema 1D (Freudenthal et al., 1998). The upper sampled levels (CY-7 and CY-8) correspond to the levels of Caravaca (De Bruijn et al., 1975; De Bruijn pers. comm.) and Almudema 1D (Freudenthal et al., 1998). To establish an age determination, a preliminary taxonomical study of the mammal fossil remains is given in this paper and a more extensive study is planned for the future. The fossil material is provisionally kept in the Department of Botany and Geology of the University of Valencia (UV). Detailed observation and photography of the fossil content were performed using a JEOL J-6510 SEM.

4. Results

The sedimentary infill of Campo Coy Basin consists of three detrital (El Chico, La Golilla and El Lobo), two evaporitic (Clavijo and Campo Coy) and one carbonate (Las Yeguas) lithostratigraphic units. We separate the lithostratigraphic units according to their position and present them according to their facies association. The results include a stratigraphic, petrological and chronological characterization for each of these units.

4.1. Lower clastic units: the El Chico and La Golilla units

4.1.1. Sedimentary facies

The El Chico Unit is the oldest stratigraphic unit and consists of 100 m of white and grey laminated marls with interbedded conglomerates and sandstones (Fig. 4). Sandstones show sheet-like, 5 to 30 cm thick, sharp-based, graded beds. In most cases, these sandstone beds show normal grading with grain size ranging from coarse-grained sand to fine sand. In some cases, the sandstone beds exhibit a basal conglomerate composed of well-rounded, pebble-sized clasts. Some sedimentary sequences are observed in the sandstones, the most complete of which begins with a basal interval of pebbles that evolves to planar laminated coarse sand and ends with medium to fine sand with hummocky and swaley cross-stratification (HCS) (Fig. 5A). Other sequences are formed by planar laminated, graded sand (Fig. 5B) or by massive sand at the base and planar lamination towards the top (Fig. 5C). Finally, some examples of sandy sequences show a lower interval of planar lamination and an upper interval dominated by oscillatory ripple cross-lamination or small-scale HCS (Fig. 5D). Conglomerate beds show small lateral continuity and are between 0.2 and 4 m thick, matrix-supported with heterometric (up to 1 m in diameter), polygenic and well-rounded clasts.

The La Golilla Unit is approximately 300 m thick, it overlies the Clavijo gypsum unit which is interstratified between the El Chico and la Golilla units, and it is composed of marls and conglomerates. The marls show similar characteristics as those of the El Chico Unit. Conglomerates are poorly sorted and clast-supported with carbonate pebbles ranging between 5 and 10 cm. These conglomerates consist of channel-like beds, generally massive, but some of them show clast imbrication or high-angle cross-stratification caused by the migration of bars within the channel. Many of the pebbles show pressure-dissolution marks. Unlike the El Chico Unit, sandstone beds are not common in this unit.

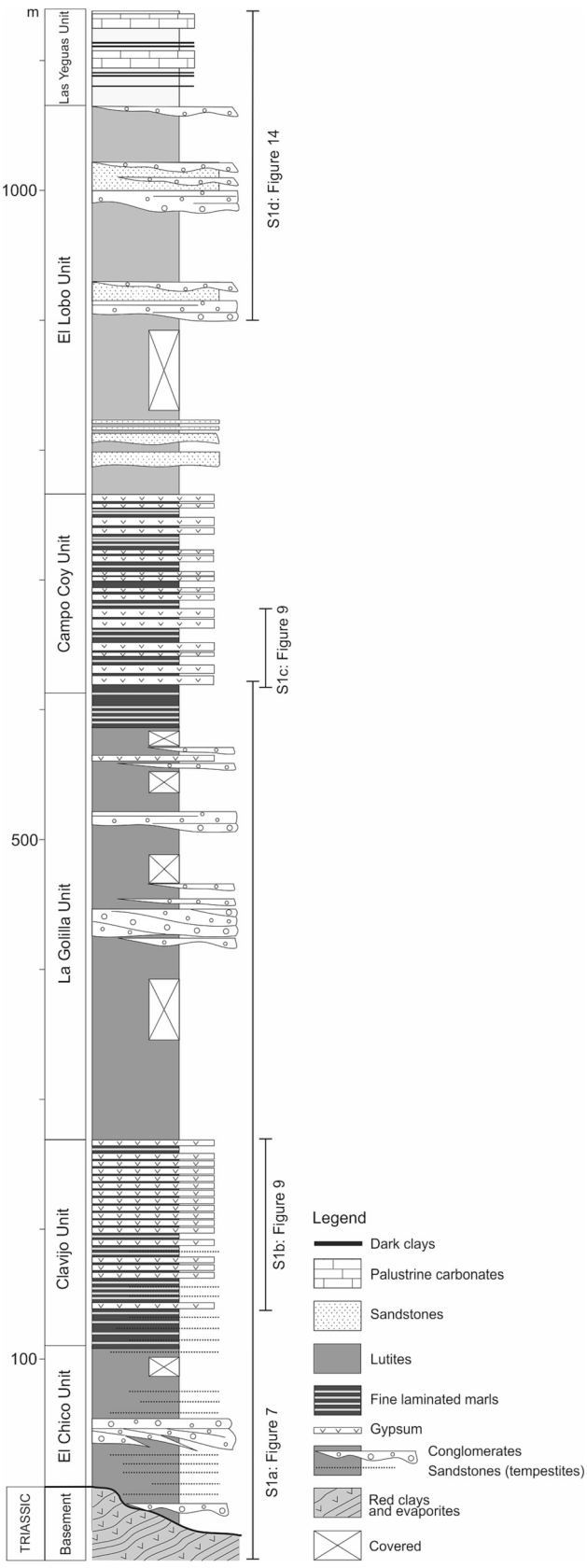

Fig. 4. Simplified stratigraphic log of the S1 section, made along the RM-711 road (See Fig. 2B).

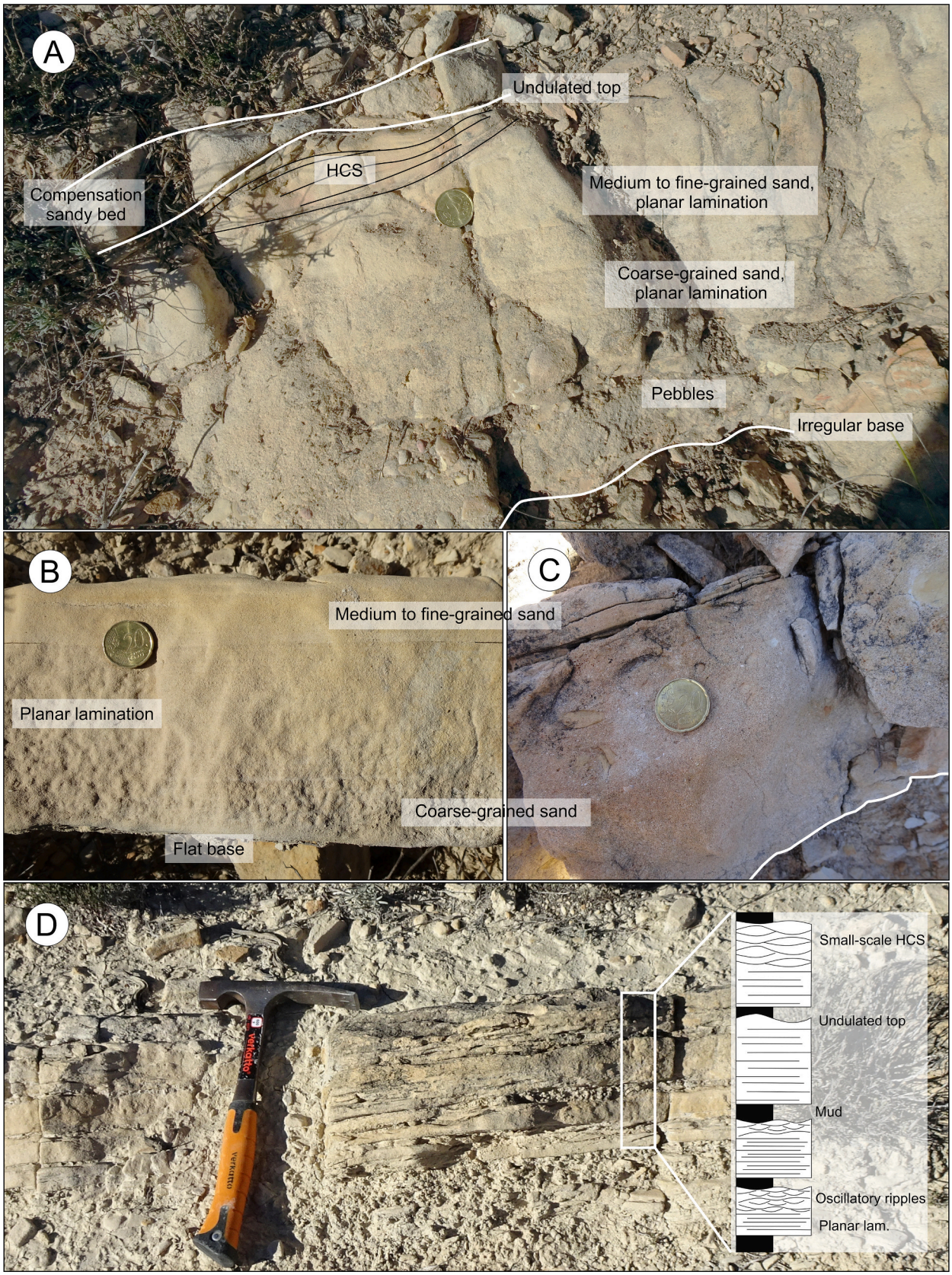

Fig. 5. Some examples of sandstone beds interpreted as lacustrine tempestites in the El Chico Unit. A) normal grading sequence with a pebble-dominated lower interval, planar lamination in the middle and hummocky-swaley cross-stratification (HCS) at the top. B, C) planar laminated or massive graded sandy sequences. D) Planar laminated thin sandstone beds topped by oscillatory ripples cross-lamination or small-scale HCS.

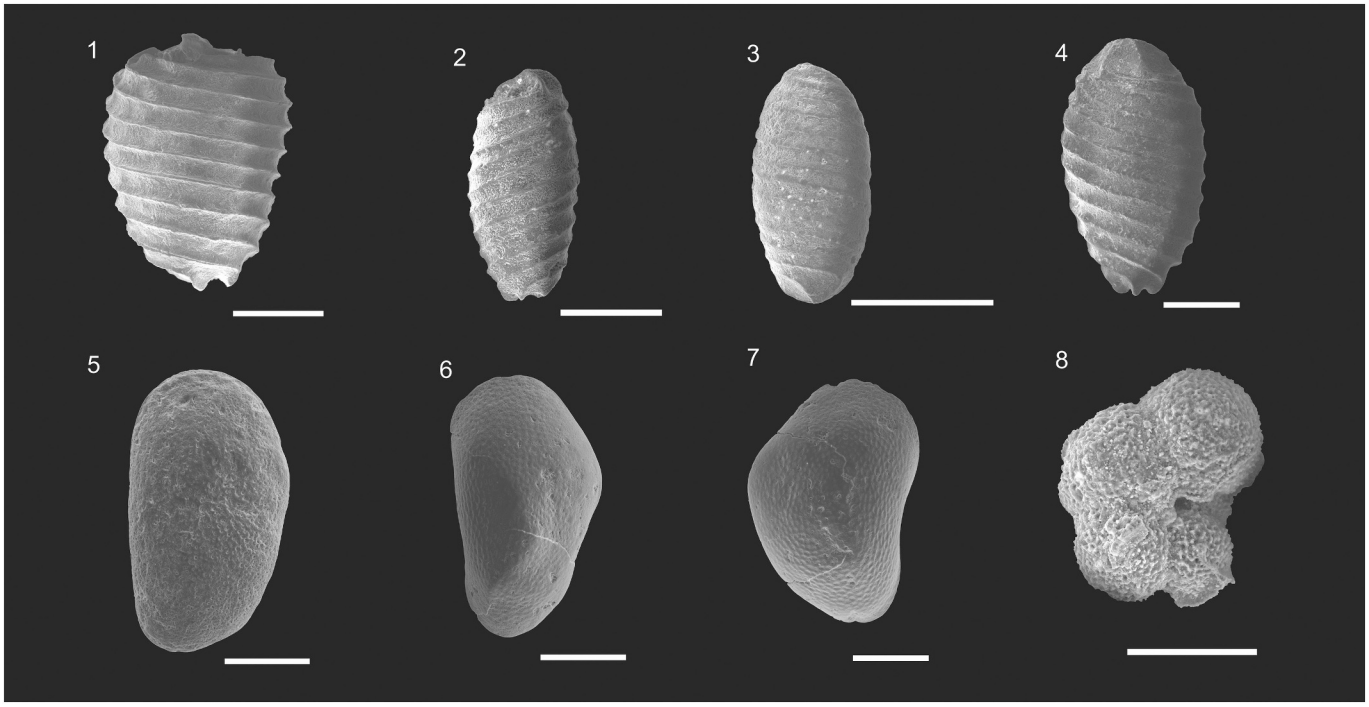

Fig. 6. Microfossil content in the El Chico and La Golilla units. 1–4) Charophyte oogonia. 5–7) Ostracods (*Cyprideis* spp.). 8) Reworked sinistral *Neogloboquadrina* sp. Scale bars = 100 μm.

4.1.2. Palaeontology

In both the El Chico and La Golilla units, the marls contain poorly preserved (reworked) planktonic and benthic foraminifera. The only well-preserved microfossils are ostracods and charophyte oogonia (Fig. 6), which represent the in situ biogenic components. The reworked foraminiferal assemblage is dominated by *Neogloboquadrina acostaensis* (dextral and sinistral coiling), *Globorotalia scitula*, *Globorotalia merotumida* and *Globorotalia menardii* (Figs. 6, 7).

4.2. The Gypsum units: Clavijo and Campo Coy

4.2.1. Sedimentary facies

The Clavijo Unit, 80 m thick, is composed of laminated gypsum alternating with carbonate laminae and marls. The boundary between the El Chico and Clavijo units is gradual. Layers of coarse-grained laminated gypsum are frequent at the base of this unit, being less common at the middle and the top of the unit where fine-grained laminated gypsum dominates. The presence of meter-scale slumps is significant, pointing to synsedimentary instability.

The Campo Coy Unit crops out along the NW-SE relief known as "Campo Coy Cordillera". It is 150 m thick and includes 8 sedimentary cycles between 15 and 20 m thick each consisting of a gypsum-dominated and a marl-dominated member. The upper cycles (4 to 8) are poorly exposed, but clearly recognizable in aerial images (Fig. 8A). The three lower cycles are well exposed (Fig. 8B), and the gypsum-dominated member of the cycles consists of gypsum interbedded with carbonates and marls. Primary gypsum dominates at the base of the gypsum cycles. In some cases, primary gypsum is replaced laterally by secondary gypsum (after anhydrite). The top of each cycle is dominated by secondary nodular and meganodular gypsum. Some gypsum layers show stromatolite-like bedding and laminated carbonates composed of micrometric subspherical dolomite aggregates occur interbedded within the gypsum layers (Fig. 8 C, D). The gypsum lithofacies of the 5 upper cycles are difficult to determine due to the poor quality of their outcrops.

The Clavijo and Campo Coy units show a variety of primary and secondary gypsum lithofacies that often display vertical and lateral changes. General features of the gypsum facies are described below, and their distribution along the units is shown in Fig. 9.

i) *Coarse-grained laminated gypsum*: Gypsum laminae and thin beds with crystal sizes ranging between 2 and 10 mm. Most of the gypsum crystals are euhedral and display subvertically aligned fabric levels (micro-selenites) (Figs. 10A, B) showing growth zoning defined by micritic inclusions.
ii) *Selenites:* Sub-vertically aligned rows of twinned crystals with the twin angle opened upward (palisade fabric). Crystal size ranges between 1 and 5 cm, distributed in beds ranging from 5 to 30 cm thick separated by thin dolomite laminae.
iii) *Nodular secondary gypsum:* Alabastrine nodules with diameters ranging between 5 and 20 cm, isolated or arranged in layers (Fig. 10C). This lithofacies also occurs as layered nodular gypsum with randomly distributed micronodules (<1 cm). Is composed of a mosaic of small, anhedral, unoriented crystals with sizes ranging between 10 and 100 μm (alabastrine texture), and with some anhydrite inclusions (Fig. 10D).
iv) *Meganodular gypsum:* Large nodules of secondary, alabastrine gypsum with diameters ranging between 30 cm and 2 m. These meganodules are distributed along the Campo Coy Unit horizontally, following the bedding and deforming the surrounding sediments (Fig. 10E). A second distribution of these meganodules is across the stratigraphy aligned along fracture zones.
v) *Gypsum laminites:* Regular alternation of cumulate fine-grained gypsum (Fig. 10F) and thin laminae of micritic carbonate, predominantly dolomite. Gypsum crystals can have lenticular or granular textures. The thickness of the gypsum laminae ranges from 1 mm to a few centimetres.
vi) *Lenticular gypsum:* Unoriented gypsum lenses of 0.1 to 5 cm in length, which occur separately and displacively between the carbonate matrix or grouped in aggregates forming a cumulate with a smaller amount of matrix.
vii) *Gypsarenites:* Levels formed by sand-sized gypsum grains accompanied by variable amounts of clastic particles (mainly quartz

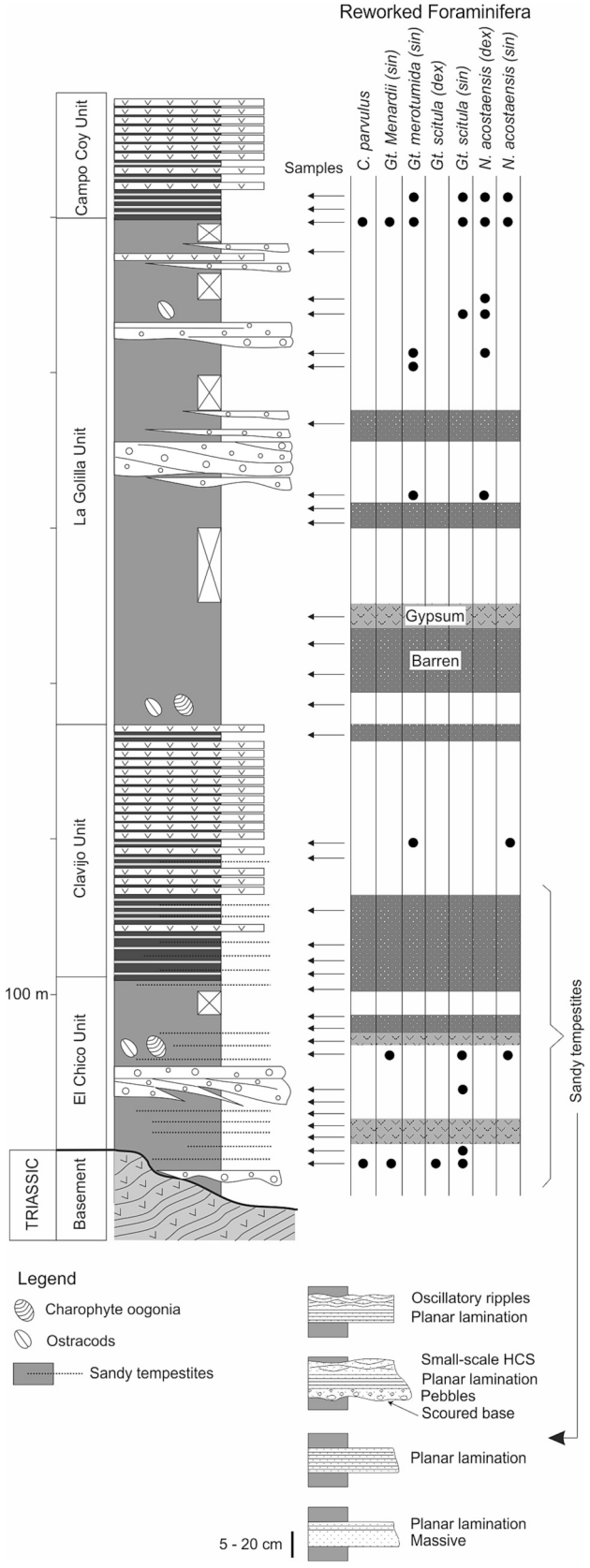

Fig. 7. Section S1a, with the indication of the reworked foraminifer species found in the studied samples, and the levels containing ostracods and Charophyte oogonia. For lithological legend, see Fig. 4.

and rock fragments), forming layers that display tractive structures such as small scale cross-bedding, parallel-bedding, current ripples, or tepee morphologies.

viii) *Macrocrystalline secondary gypsum*: Contrary to the other secondary gypsum facies, this gypsum does not show an alabastrine texture as it is composed of a mosaic of big (0.3 to 2 cm), transparent crystals showing some anhydrite remains inside (Fig. 10G). The thickness of these gypsum beds ranges between a few cm to 1 m.

ix) *Convolute gypsum:* Levels of secondary alabastrine gypsum, strongly folded and deformed, mainly found at the top of the gypsum cycles in the Campo Coy Unit. The levels are between 1 and 10 cm thick (Fig. 10H).

x) *Bioturbated gypsum:* Consist of massive, brownish gypsum layers up to 1 m thick. It is composed of lenticular to anhedral crystals ranging between 50 and 500 μm in size, forming a crystal-supported mosaic with variable amounts of micritic matrix. The presence of bioturbation (burrows) is common in these lithofacies (Fig. 10I).

4.2.2. Gypsum isotopy

The sulphur ($\delta^{34}S$) and oxygen ($\delta^{18}O$) isotopic compositions of the gypsum from the Clavijo and Campo Coy units show homogenous values. The $\delta^{34}S$ values range from +11‰ to +15.6‰ V-CDT. The $\delta^{18}O$ compositions range from +13.8‰ to +18.7‰ V-SMOW (Fig. 11, Supplementary table S2). The strontium isotope ratios ($^{87}Sr/^{86}Sr$) show values between 0.707788 and 0.707888, matching the range of Triassic marine evaporites (Table 1).

4.3. The upper units: El Lobo and Las Yeguas units

4.3.1. Sedimentary facies

The El Lobo Unit is formed, at the base, by loams and abundant sandstone beds showing planar and cross-stratification. It is approximately 300 m thick in S1. The upper 200 m consists of a succession of conglomerates, reddish lutites and sandstones. Conglomerates are heterometric and clast supported, composed of carbonate pebbles and with a sandy-loam matrix between clasts. These conglomerates usually show an erosive surface and form channel-like beds (Fig. 12A, B). To the west, the unit thickness decreases, and the materials laterally change to massive white marls showing bioturbation.

The El Lobo Unit grades upwards into the Las Yeguas Unit (50 m thick), composed of brownish and whitish lutites, silts, carbonates and abundant fossiliferous dark clay layers (Fig. 12 C, D). This upper interval contains abundant gastropods and has evidence of pedoturbation. Carbonates are nodular and highly compacted, mainly composed of calcite and partially silicified.

4.3.2. Magnetostratigraphy

The studied samples have been classified according to the quality with which the primary magnetization is recorded. First-class samples display demagnetization patterns where all measured specimens show consistent normal or reverse primary directions, allowing an unambiguous interpretation of the characteristic remanent magnetization (ChRM) (Fig. 13). Second-class samples usually have weak magnetization, but the secondary components can be removed during the demagnetization process allowing to isolate the primary direction in at least one specimen. The third-class samples are usually poorly magnetized, primary and secondary components cannot be separated during demagnetization and their ChRM direction cannot be determined. Approximately 45% of the samples are first-class, usually associated with reddish lutites, and 26% of the samples belong to the second-class group. The rest of the samples have been classified as third-class and most of them are located in the carbonates of the Las Yeguas Unit. Only the first and second class samples have been used to interpret the local polarity sequence, which consists of 6 magnetic reversals defining 3

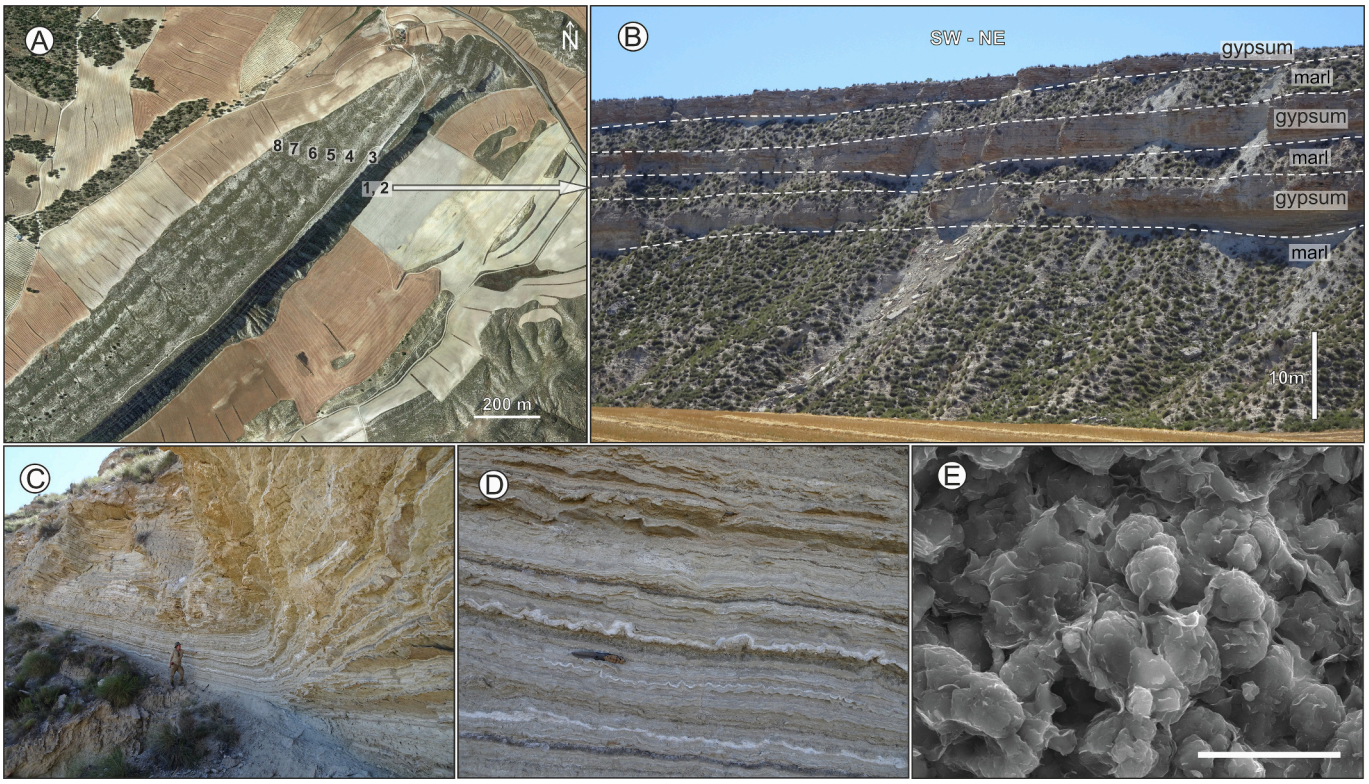

Fig. 8. Campo Coy Unit A) Satellite image of the Campo Coy Cordillera, in which the 6 upper gypsum cycles of the Campo Coy Unit (3 to 8) can be clearly distinguished. The gypsum corresponds to the whitish intervals, while the marls are marked by the greenish intervals due to the vegetation cover. B) South face of the Campo Coy Cordillera, in which the 3 lower gypsum cycles of the Campo Coy Unit can be distinguished. C) Outcrop view of the first gypsum cycle of the Campo Coy Unit. D) Stromatolite-like bedding between the gypsums and carbonates. E) SEM image of a dolomicrite sample, composed of dolomite spheroids.

normal (N1 to N3) and 4 reverse magnetozones (R1 to R4) (Fig. 14).

4.3.3. Palaeontology

The 8 sampled dark claystone levels of the Las Yeguas Unit (CY-1 to CY-8) show a rich micromammal (rodent) fossil content (Figs. 15, 16). This palaeontological study supplies biostratigraphic information to anchor the identified polarity sequence to the Global Polarity Time Scale (GPTS) and dates the upper 250 m of the sequence. As a group, the fossil assemblage is composed of 22 species representing 15 genera, including some African immigrant genera such as *Paraethomys* spp. and *Debruijnimys* sp., although in the case of *Debruijnimys,* the presence of only a fragmentary tooth does not allow a precise specific attribution. The fossil association and its distribution along the studied section are shown in Fig. 16.

4.3.4. Carbonate isotopy

Stable isotopes ($\delta^{18}O$ and $\delta^{13}C$) from all calcite samples from the Las Yeguas Unit show negative isotopic values ranging between −8.67 and − 5.82 for $\delta^{13}C$ and between −7.22 and − 5.19 for $\delta^{18}O$ (Fig. 17).

5. Discussion

5.1. Sedimentary environments

The presence of ostracods and charophytes in the El Chico and La Golilla units, together with the absence of in situ marine fossils, indicates that the sedimentation of these units took place in a lacustrine environment as in the nearby Baza Basin (Gibert et al., 2007). The sandstone beds described in the El Chico Unit (see Fig. 5) can be interpreted as sandy tempestites, adopting the storm-ebb surges model (Cheel, 1991). These deposits develop in lakes with sandy and gravel shores, which are the source of sediment for the deposition of the tempestites during storm events (Uchman et al., 2007).

Gypsum has a sulphur, oxygen and strontium isotopic composition similar to the brine from which it has precipitated. The isotopic values of $\delta^{34}S$, $\delta^{18}O$ and $^{87}Sr/^{86}Sr$ from the studied gypsums show the typical isotopic signature expected for Triassic marine sulphates (McArthur et al., 2012; Ortí et al., 2014; Ortí et al., 2022) (See Fig. 16, Table 1). No Miocene marine or mixed isotopic values have been reported in the studied samples, so marine water input to the basin should be discarded. The most plausible source of sulphate to the basin is the recycling of the nearby Triassic evaporites, which would have been transported to the basin through the rivers and groundwaters in a continental setting.

In the Clavijo Unit, the predominantly laminated gypsum lithofacies and the absence of cyclicity or subaerial exposure evidence, suggest a relatively deep (meters or tens of meters) perennial lacustrine environment (Warren, 2006). This hypothesis is consistent with the presence of meter-scale slumps, which indicates an important bathymetric gradient in the basin. The nodular secondary gypsum in this unit along the S2 section is associated with fractures of approximate N-S orientation and would thus be related to the circulation of anhydritizing hypersaline fluids through the fractures, in a similar process to the formation of meganodules in the Calatayud basin, Spain (Ortí and Rosell, 2000; Ortí et al., 2010). The hypersaline fluids would come from the Triassic salts located at shallow depths. An example of hypersaline springs occurs today in the Periago saltwork, located in the southernmost part of the basin.

The Campo Coy Unit shows a shallower environment than the Clavijo Unit, as its deposits are characteristic of a shallow ephemeral gypsiferous lake in which a sequence of shallowing and increasing salinity is recorded from base to top of each cycle, similar to the case of the "sabkha cycles" described in the Calatayud Basin (Ortí and Rosell, 2000). At the top of each cycle, primary anhydrite formed in hypersaline sabkha-like environments and was subsequently hydrated and

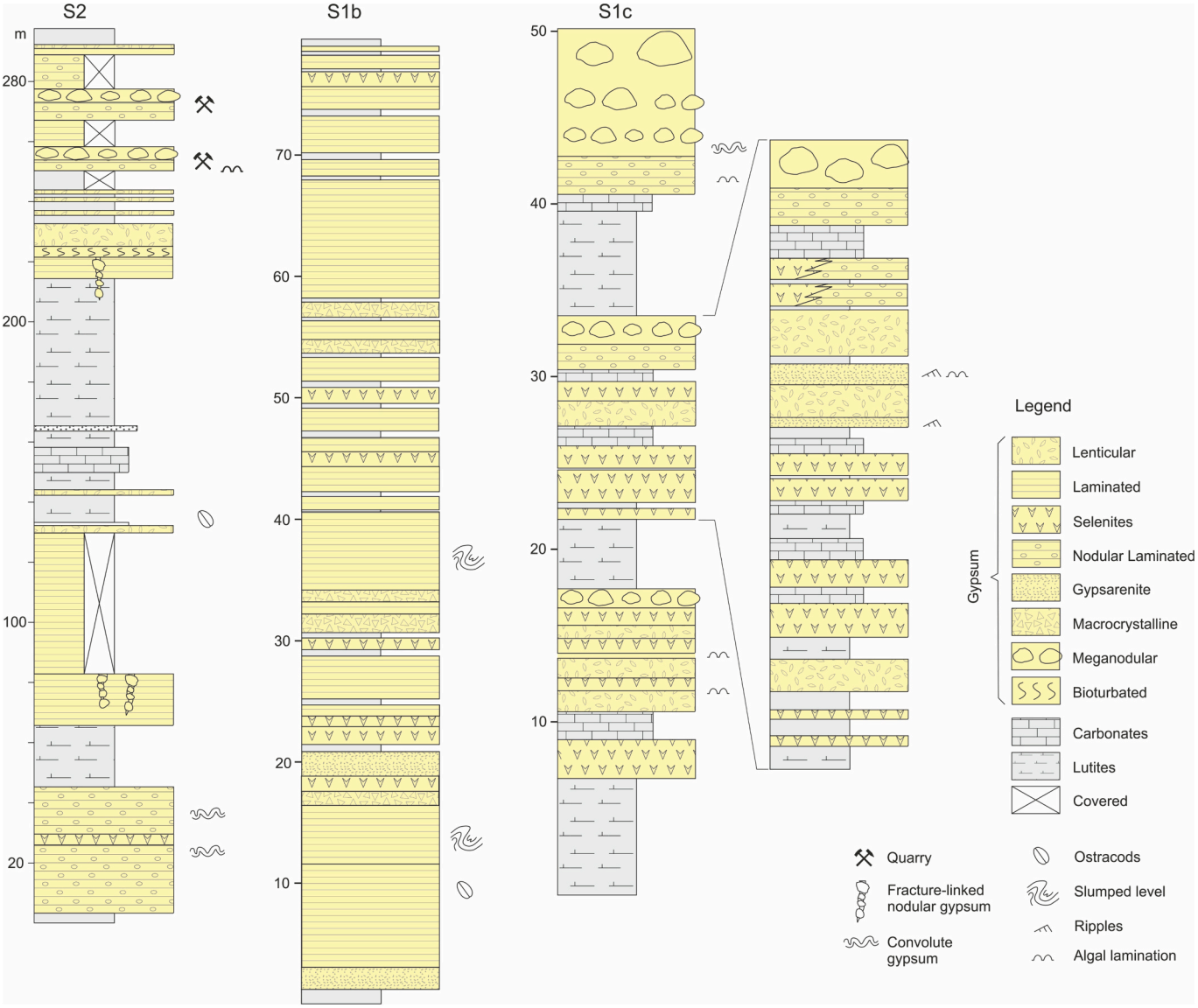

Fig. 9. Stratigraphic sections showing the distribution of the gypsum lithofacies.

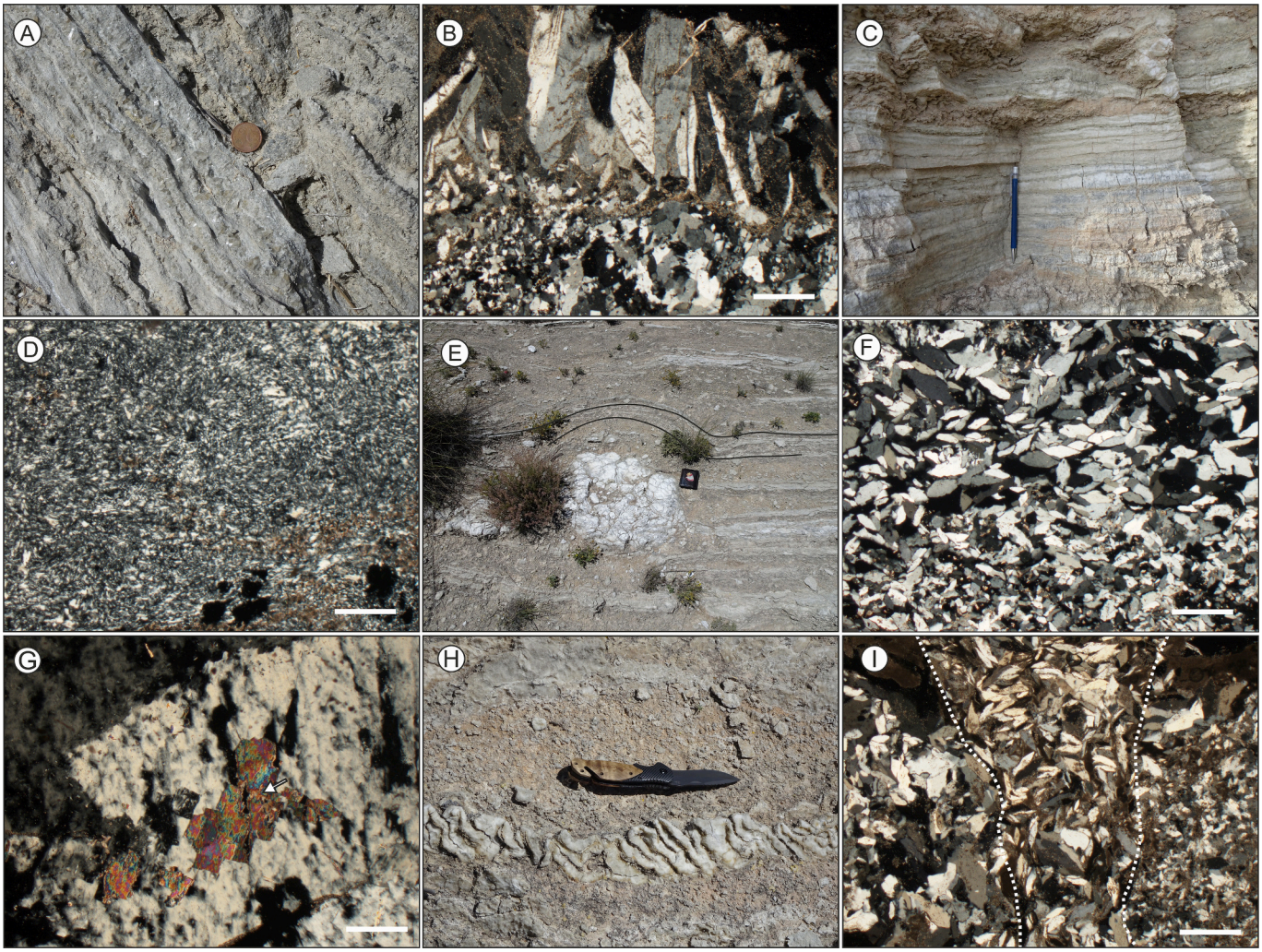

Fig. 10. Gypsum facies. A) Coarse-grained laminated gypsum, with some layers of vertically oriented crystals (small selenites). B) Fine-grained gypsum laminae under a selenite layer separated by a micrite horizon. C) Laminated nodular gypsum. D) Microcrystalline alabastrine texture of a gypsum nodule. E) Alabastrine gypsum nodule deforming the overlying layers. F) Laminated gypsum layer composed of lenticular crystals with a cumulate texture and reverse gradation. G) Macrocrystalline gypsum with anhydrite relicts in the centre. H) Convolute gypsum layer. I) Bioturbated gypsum. The dashed lines limit a burrow that contains lenticular crystals and a higher matrix proportion than the surrounding material. Scale bars in the photomicrographs are equal to 0.5 mm.

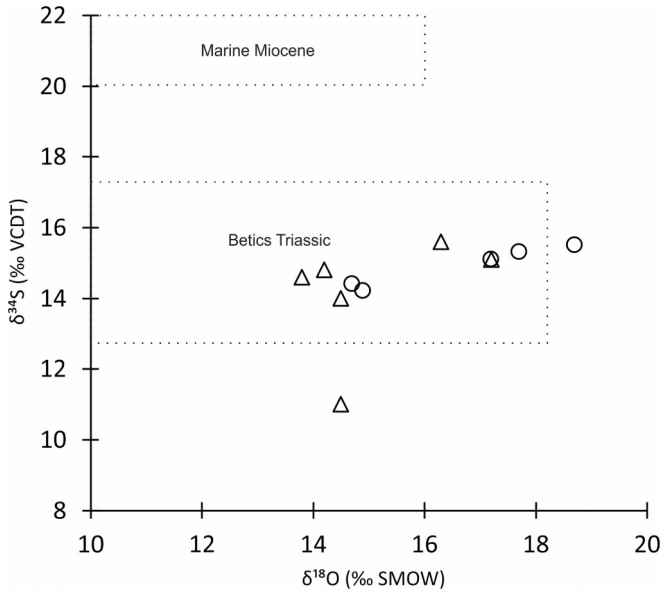

Fig. 11. Oxygen and sulphur isotopic composition of the gypsums in the El Chico Unit (triangles) and Campo Coy Unit (circles). The dashed rectangles represent the expected value ranges for Triassic sulphates (Ortí et al., 2022) and for Late Miocene marine sulphates (Claypool et al., 1980).

Table 1
Strontium isotope ratios ($^{87}Sr/^{86}Sr$) from Campo Coy basin gypsum compared with published database strontium values (Henderson et al., 1994; McArthur et al., 2012; Ortí et al., 2014).

Unit	Source	$^{87}Sr/^{86}Sr$
Campo Coy Unit		0.707817
Campo Coy Unit		0.707888
Campo Coy Unit		0.707788
Clavijo Unit		0.707854
Clavijo Unit		0.707868
	Late Miocene sea water	0.708983–0.709028
	Triassic marine evaporites	0.707615–0.708114
	Present day ocean water	0.709155

transformed into secondary gypsum during dilution episodes. The shallow environment is also supported by the presence of crenulated beds with gypsum and dolomite. This dolomite shows subspherical aggregate crystals suggesting primary bacterially induced dolomite (e.g. Sánchez-Román et al., 2008, 2009, 2011; Balci and Demirel, 2016). Similar dolomite has been reported in the nearby Late Miocene Las Minas Basin (Lindke et al., 2011; Pineda et al., 2021). Therefore, the discrete convoluted and crenulated gypsum beds and associated dolomite may be related to gypsified microbial mats. The gypsum meganodules are deforming the overlying lamination as shown in Fig. 10E, suggesting an early diagenetic formation, in which interstitial primary anhydrite precipitated replacing the previous gypsum lithofacies (Salvany and Ortí, 1990). However, the diagenetic anhydritization from hypersaline fluids is also evident in this unit considering the lateral changes of primary to secondary gypsum. The massive bioturbated gypsum is also related to a shallow lacustrine environment. Burrowing is produced by small insects and annelids during episodes of relative dilution along the lake margin. In the Calatayud and Teruel basins, these facies have been interpreted as formed in palustrine gypsiferous settings (Rodriguez-Aranda and Calvo, 1998; Ortí and Rosell, 2000; Ortí et al., 2003).

The 8 decametric evaporitic cycles observed in the Campo Coy Unit (Figs. 8, 10) have a very similar thickness and a relevant lateral continuity (>10 km). Because tectonic processes are not cyclic at the time scale represented in the Campo Coy Unit, the origin of these cycles should be attributed to climatic fluctuations (wet/dry periods) related to insolation cycles derived from the Earth's orbital parameters. Precessional cycles of similar age controlled the sedimentation in the nearby marine Sorbas basin with cycles ranging from 1 to 2 m (Abad marls) to 8–29 m thick for the evaporites of the Yesares member (Krijgsman et al., 1999; Krijgsman et al., 2001). However, with the available data, it is not possible to assign a specific orbital periodicity (Precession, Obliquity, or Eccentricity) to the Campo Coy cycles.

The reddish sediments of the El Lobo Unit are interpreted as alluvial fan deposits on the margin of a playa lake system, while the Las Yeguas Unit is interpreted as a shallow lacustrine to palustrine environment. The low carbon and oxygen isotopic values in the Las Yeguas carbonates (see Fig. 17) suggest important freshwater inputs in an open lake during a wet period (Talbot, 1990). According to the evolution of the sedimentary facies, the El Lobo Unit was formed in a relatively arid period that evolved into a wetland represented by the Las Yeguas Unit (see Fig. 14).

5.2. *Biochronology and palaeomagnetic dating*

The fossil content of the Las Yeguas Unit shows characteristic species of the MN14 Mammal Neogene Zone, corresponding to the Ruscinian land mammal age, and some species of the lower levels could be assigned to the MN13 zone (Ventian age). The Ventian stage (Aguirre et al., 1976), includes the Spanish faunas assigned to the MN13 and ends with the appearance of *Promimomys* at ca. 5 Ma (Morales et al., 2013) (See Supplementary Fig. S1). The presence of *Apocricetus barrierei* or *Apocricetus* cf. *barrierei, Paraethomys baeticus* and *Occitanomys brailloni* in the time span represented between levels CY-3 and CY-8 allows us to assign a Pliocene age (MN-14 zone, Ruscinian) to this part of the Las Yeguas Unit (Mein et al., 1990; Freudenthal et al., 1998; Kälin, 1999; García-Alix et al., 2008a, 2008b; Ruiz-Sánchez et al., 2014; Mansino et al., 2015, 2017a; Piñero and Agustí, 2019). Only levels CY-1 and CY-2 do not contain clear Pliocene species. Nevertheless, *Apocricetus* sp. from the sample CY-2 (Fig. 15) would be assigned to *Apocricetus barrierei* or *Apocricetus* cf. *barrierei,* but scarce and deteriorated material from this taxon led us to assign it only to genus level. With respect to the record of *Paraethomys meini* in the sample CY-1 and *Apodemus gudrunae* in CY-4, these species are characteristic of both MN-13 Ventian (Mansino et al., 2017b) and Ruscinian (García-Alix et al., 2008a; Mansino et al., 2013; Piñero et al., 2017). The presence of African immigrants such as *Paraethomys* spp. and *Debruijnimys* sp. was cited by de Bruijn et al. (1975) for the site of Caravaca, which corresponds to the uppermost fossiliferous layer (CY-8) (de Bruijn pers. comm.) and is confirmed in this study. The migration of gerbils to Europe occurred during the MSC (Gibert et al., 2013) and extends to the Pliocene.

The micromammal fossil assemblage allows us to establish a correlation between the local magnetic polarity sequence and the Geomagnetic Polarity Time Scale (GPTS, Gradstein et al., 2012). Considering the time span of the MN14 biozone (~5 to 4.2 Ma after Morales et al., 2013), we propose the correlation shown in Fig. 14. The S1d section would comprise a period between approximately 6.4 and 4.7 Ma. This interpretation implies that the El Lobo Unit is coeval to the Messinian Salinity Crisis (5.9 to 5.33 Ma) (Van Couvering et al., 2000; Manzi et al., 2013).

The age of the rest of the sedimentary record is more difficult to determine because no in situ microfossils have been found and palaeomagnetic data is neither available. Nevertheless, we can estimate a maximum age for the El Chico and La Golilla units considering the content of reworked foraminifera and, consequently, a maximum age for the basin. The abundant presence of reworked sinistral forms of *Neogloboquadrina acostaensis* opens two options for their maximum age (Lirer et al., 2019, and references therein): 1) a first dextral/sinistral shift at 10.05 Ma. This event of the dominant presence of sinistral forms is very short (10.05–9.90 Ma) and consequently it is unlikely to find abundant reworked material from this period. 2) A second and much

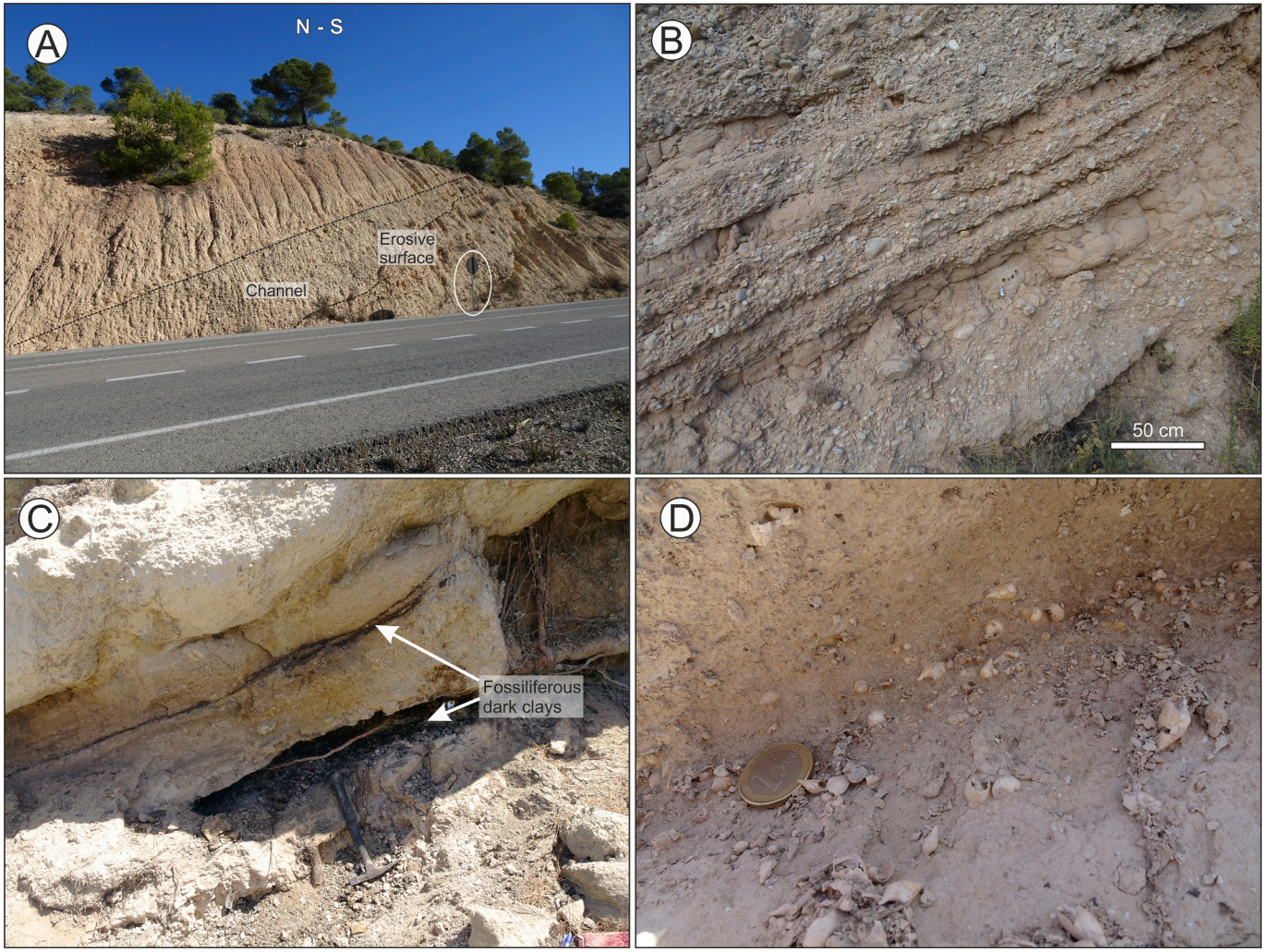

Fig. 12. A, B) Conglomerates and reddish clays of the El Lobo Unit. C) Gastropod-rich level of the Las Yeguas Unit. D) Dark fossiliferous clay levels in the Las Yeguas Unit. The lower one corresponds to CY-1.

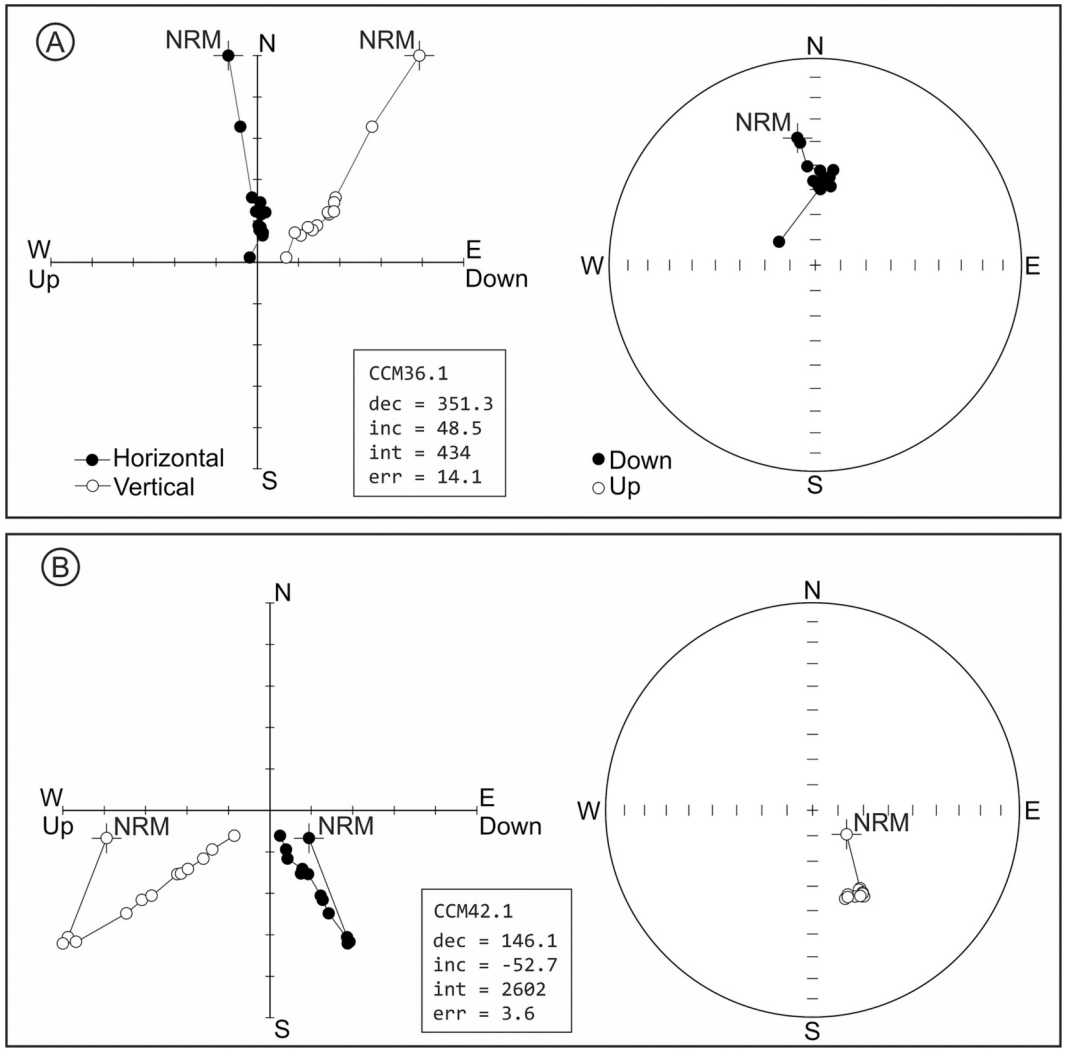

Fig. 13. Thermal demagnetization diagrams of selected Class I samples. Zijderveld diagrams to the left and stereographic plots to the right. A) Normal polarity. B) Reverse polarity.

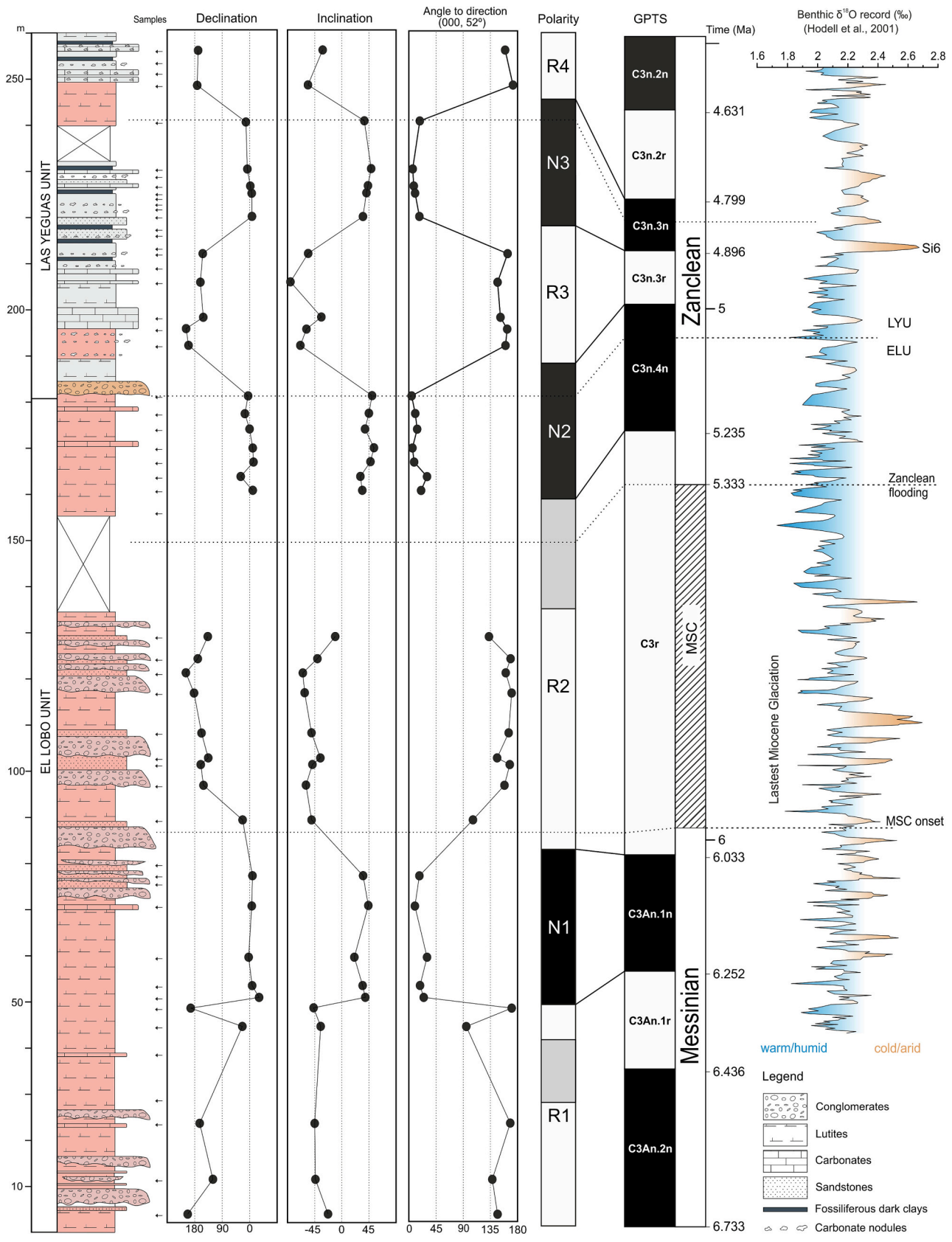

Fig. 14. S1d section representing the upper half of the El Lobo and Las Yeguas Unit, with the composite magnetostratigraphy of the section and the proposed correlation with the Geomagnetic Polarity Time Scale (GPTS) (Gradstein et al., 2012). The Messinian Salinity Crisis time-lapse is shown in the GPTS. Data are provided in declination, inclination and the angle (Δ) to the expected normal direction (000, 52) (after Hoffman, 1984). The colours in the column represent the colour tones of the outcropping lithologies.

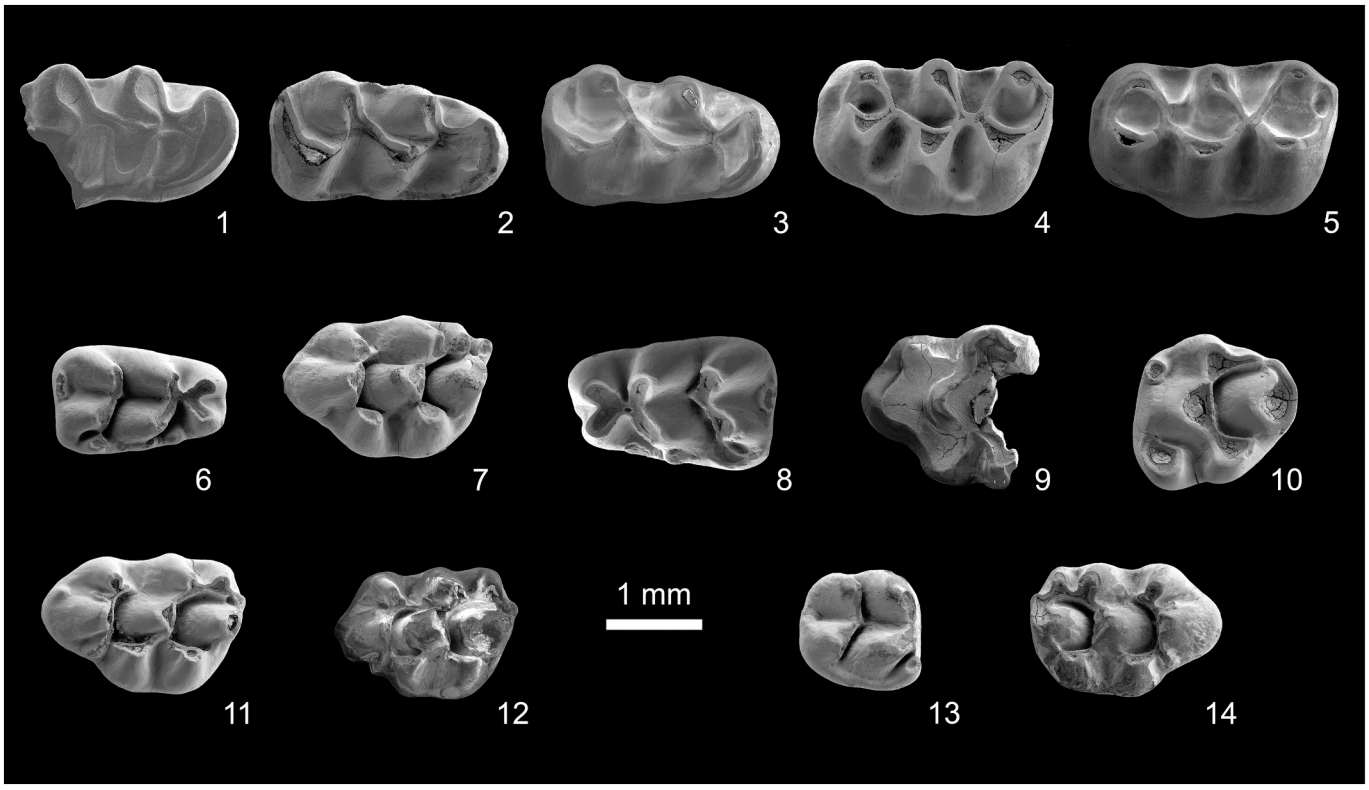

Fig. 15. Micromammal assemblage found in Las Yeguas Unit. *Apocricetus* sp.: 1, right m1 (CY2–1); *Apocricetus* cf. *barrierei*: 2, right m1 (CY3–1); *Apocricetus barrierei*: 3, right m1 (CY8–1); 4, left M1 (CY7–12); 5, left M1 (CY8–4); *Paraethomys meini*: 6, right m1 (CY1A-1); *Paraethomys* cf. *meini*: 7, left M1 (CY2–4); *Paraethomys baeticus*: 8, left m1 (CY8–9); 9, left M1 (CY8–29); *Paraethomys* cf. *baeticus*: 10, left M2 (CY6–19); *Occitanomys brailloni*: 11, left M1 (CY6–14); 12, left M1 (CY6–15); 13, right m2 (CY7–35) and 14, right M1 (CY7–51). Scale bar equals 1 mm.

longer dextral/sinistral shift at 9.54 Ma, which extends through the rest of the Tortonian and much of the Messinian (up to 6.35 Ma) and has been used to separate the Mediterranean biostratigraphic zone MMi11 into the subzones MMi11a and MMi11b (Corbí and Soria, 2016). Therefore, we can assume that the studied reworked material is older than this second event, so, the presence of reworked sinistral *N. acostaensis* indicates that, at the time of the sedimentation of the El Chico Unit, emerged middle Tortonian materials existed nearby and were being eroded by rivers that discharged their waters into the ancient Campo Coy Lake. These middle Tortonian materials, which would most likely form part of the basin basement, limit the age of the basal deposits to younger than 9.54 Ma. That basement, to be lifted and eroded, must have taken at least several hundred thousand years, so it is logical to assume an age of approximately 9 Ma as the maximum age for the Campo Coy Basin.

5.3. Implications for the Betic Seaway and the Messinian Salinity Crisis

In the context of the Betic Seaway, the Campo Coy Basin was in an intermediate position between two main marine Basins: The Guadix-Baza Basin and the Lorca Basin. The continentalization of the Guadix-Baza Basin dates from the latest Tortonian, about 7.8 Ma (Soria et al., 1999), while the continentalization age of the Lorca Basin is controversial ranging from 7.6 to 6 Ma (Krijgsman et al., 2000; García-Veigas et al., 2019; Carpentier et al., 2020). Indeed, the Campo Coy Basin must have been a connection between Guadix-Baza and Lorca during the Serravalian-early Tortonian as indicated by the marine sediments of the Campo Coy basement (Baena, 1974; Paquet et al., 1974). The maximum age of the base of the sedimentary succession studied here, according to the reworked microfossils, suggests that the continentalization of the basin took place most probably during the middle Tortonian, later than 9 Ma. This age would imply that the Guadix-Baza and Lorca basins were disconnected from each other around that time. Lorca remained connected to the Mediterranean and Guadix-Baza to the Atlantic with a possible connection to the Mediterranean through the Almanzora corridor (Fig. 18). The alluvial deposits of the El Lobo Unit are coeval with MSC, indicating a dry and cold continental environment during the restriction of the Mediterranean coincident with the Latest Miocene Glaciation (Hodell et al., 2001) (See Fig. 14). Our results show that after ~5.1 Ma, these alluvial deposits gradually changed to the lacustrine carbonates of the Las Yeguas Unit. This gradual change from alluvial to lacustrine sedimentation gently starts at the upper part of the El Lobo Unit with the occurrence of the first carbonate beds and the decrease of detrital deposits, suggesting that a change towards wetter conditions followed the end of the MSC. The change from alluvial to lacustrine facies around the Messinian-Zanclean transition is similar to the one described in the continental MSC-contemporary Kumarlı section in central Anatolia (Meijers et al., 2018), which shows a decrease in conglomerate deposits just after the end of the MSC, although its stratigraphic record is not described in detail (see Supplementary Fig. S2). Our results agree with previous studies that have proposed a dryer climate than today in the circum-Mediterranean region during the MSC, followed by an increase in humidity at the early Zanclean (Kayseri-Özer, 2017; Vasiliev et al., 2017; Meijers et al., 2018). Episodes of colder temperatures could be related to the presence of reddish clay intervals between the lacustrine deposits of the Las Yeguas Unit (see Fig. 14).

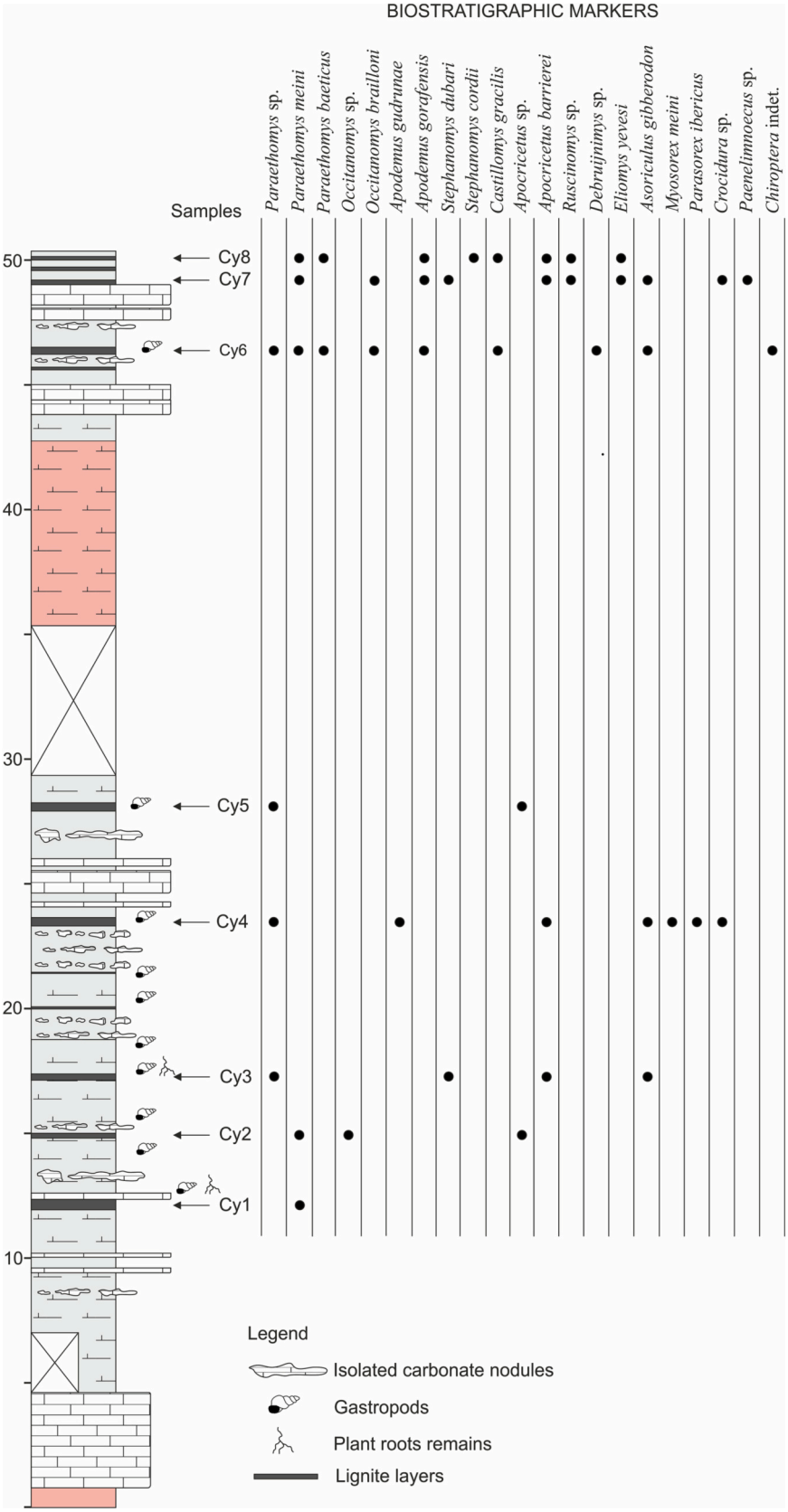

Fig. 16. Stratigraphic log of the Las Yeguas Unit, with the location of the collected micromammal samples (dark clays) and the distribution of the fossil assemblage. See Fig. 14 for lithological legend. The colours in the column represent the colour tones of the outcropping lithologies.

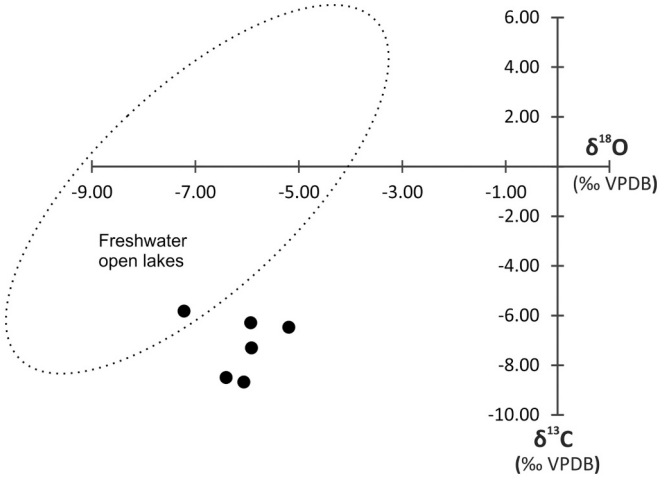

Fig. 17. Stable carbon and oxygen isotope compositions of the carbonates in the Las Yeguas Unit. The dashed area marks the expected values for freshwater open lakes (Talbot, 1990).

6. Conclusions

The infill of the Campo Coy Basin is formed by six lithostratigraphic units which constitute a continental record that precedes, covers and postdates the Messinian Salinity Crisis of the Mediterranean. The pre-MSC deposits are represented by lacustrine siliciclastic materials formed in a shallow sandy-shore lake, containing reworked middle-Tortonian foraminifera (El Chico Unit). The Clavijo and Campo Coy units represent two gypsiferous lake environments, with hypersaline episodes developed during the driest periods in the case of the Campo Coy Unit. Isotopic values of the gypsum ($\delta^{34}S$, $\delta^{18}O$, $^{87}Sr/^{86}Sr$) indicate that gypsum formed after the chemical recycling of the Triassic evaporites. Secondary gypsum in these units formed 1) during the early diagenesis in continental hypersaline environments, and 2) during the late diagenesis due to the circulation of hypersaline fluids through fractures. The alluvial deposits of the El Lobo Unit suggest a dry environment developed during the MSC and represent the first described continuous continental record that covers the MSC in the western Mediterranean. The lacustrine carbonates of Las Yeguas Unit directly postdate the MSC and were formed in an open lake with important freshwater inputs during a wet period. This unit is rich in micromammal remains including African immigrant species that crossed to Europe through ephemeral land bridges generated during the MSC. The palaeomagnetic study of the El Lobo and Las Yeguas units, together with the micromammal biomarkers allows us to constrain the age of the upper part of the studied sequence between 6.4 and 4.7 Ma. The reworked foraminifera biomarkers of the El Chico and La Golilla units allow us to establish a maximum age of 9 Ma for the sedimentary record of the Campo Coy Basin. This new sedimentological and chronostratigraphic information indicates that this area was already isolated from the sea during the late Tortonian and that the neighbouring basins of Guadix-Baza and Lorca were disconnected from each other before 9 Ma.

Supplementary data to this article can be found online at https://doi.org/10.1016/j.palaeo.2023.111424.

Declaration of Competing Interest

The authors declare that they have no known competing financial

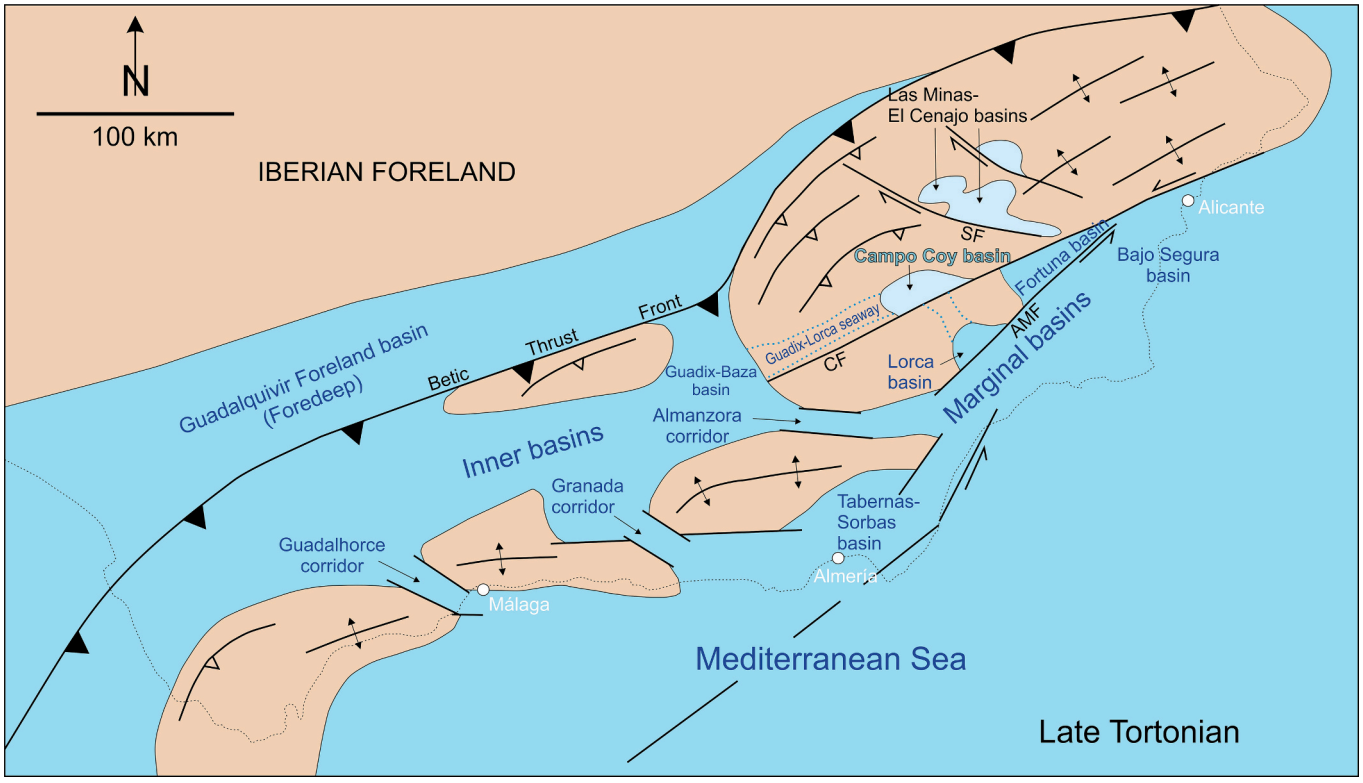

Fig. 18. Palaeogeographic reconstruction of the Betic Seaway during the late Tortonian, with the location of the continental Campo Coy Basin. Note that there is not a direct seaway between Guadix-Baza and Lorca Basins. The blue dashed line marks the position of the previously proposed seaway between Guadix and Lorca basins (Soria et al., 1999; Corbí et al., 2012). (Modified from García-Veigas et al., 2019; Pineda et al., 2021). CF: Crevillente Fault; AMF: Alhama de Murcia Fault. (For interpretation of the references to colour in this figure legend, the reader is referred to the web version of this article.)

interests or personal relationships that could have appeared to influence the work reported in this paper.

Data availability

Data will be made available on request.

Acknowledgments

To the memory of Hans de Bruijn, who explore the Campo Coy Basin in the early seventies and kindly provided us with information about the vertebrate fossils he discovered. Thanks to Dioni Cendón for the help with the radiogenic Sr measurements, to Elisabet Beamud from the Palaeomagnetism Laboratory of the GEO3BCN-CSIC and to the anonymous reviewers who helped to improve this manuscript. Funding was provided by the grants CGL-2016-79458 and PID2020-118999GB-I00 from the Spanish Ministry of Science and Innovation (MCIN)/ State Research agency of Spain (AEI)/10.13039/501100011033, and by the Catalonian Government Actions 21-SGR-829 and PGC2018-094122-B-100.

References

Aguirre, E., López, N., Morales, J., 1976. Continental faunas in Southeast Spain related to the Messinian. In: Cita, M.B. (Ed.), Il significato geodinamico della crisis di Salinita del Miocene Terminale nel Mediterraneo. Messinian Seminar N. 2, Gargano, pp. 62–63.

Andrieux, J., Fontboté, J.M., Mattauer, M., 1971. Sur un modele explicatif de l'Arc de Gibraltar. Earth Planet. Sci. Lett. 12, 191–198.

Artiaga, D., García-Veigas, J., Gibert, L., Soria, J.M., 2020. The late Miocene Campo Coy gypsum (Eastern Betics, Spain). Geogaceta 67, 63–66.

Baena, J., 1974. Mapa geológico y memoria de la hoja n° 931 (Zarcilla de Ramos). In: Mapa Geológico de España E. 1:50000. Segunda Serie (MAGNA), Primera edición. IGME.

Balci, N., Demirel, C., 2016. Formation of carbonate nanoglobules by a mixed natural culture under hypersaline conditions. Minerals 6, 122.

Butler, R.F., 1992. In: Paleomagnetism: Magnetic Domains to Geologic Terranes. Blackwell Scientific Publications, Boston, p. 238.

Carpentier, C., Vennim, E., Rouchy, J.M., Cornée, J.J., Melinte-Dobrinescu, M., Hibsch, C., Olivier, N., Caruso, A., Bartier, D., 2020. Ages and stratigraphical architecture of late Miocene deposits in the Lorca Basin (Betics, SE Spain): New insights for the salinity crisis in marginal basins. Sediment. Geol. 405, 105700.

Chalouan, A., Michard, A., Feinberg, H., Montigny, R., Saddiqi, O., 2001. The Rif mountain building (Morocco); a new tectonic scenario. Bull. Soc. Géol. France 172, 603–616.

Cheel, R.J., 1991. Grain fabric in hummocky cross-stratified storm beds: genetic implications. J. Sediment. Petrol. 61, 102–110.

Claypool, G.E., Holser, W.T., Kaplan, I.R., Sakai, H., Zak, I., 1980. The age curves of sulfur and oxygen isotopes in marine sulfate and their mutual interpretation. Chem. Geol. 28, 199–260.

Colom, G., 1952. Aquitanian-Burdigalian diatom deposits of the North Betic Strait, Spain. J. Paleontol. 26, 867–885.

Corbí, H., Lancis, C., Garcia-Garcia, F., Pina, J.A., Soria, J.M., Tent-Manclus, J.E., Viseras, C., 2012. Updating the marine biostratigraphy of the Granada Basin (central Betic Cordillera). Insight for the late Miocene palaeogeographic evolution of the Atlantic-Mediterranean seaway. Geobios 45, 249–263.

Corbí, H., Soria, J.M., Lancis, C., Gianneti, A., Tent-Manclús, J.E., Dinarès-Turell, J., 2016. Sedimentological and paleoenvironmental scenario before, during, and after the Messinian Salinity Crisis: the San Miguel de Salinas composite section (western Mediterranean). Mar. Geol. 379, 246–266.

Corbí, H., Soria, J.M., 2016. Late miocene–early Pliocene planktonic foraminifer event-stratigraphy of the Bajo Segura basin: a complete record of the western Mediterranean. Mar. Pet. Geol. 77, 1010–1027.

Crespo-Blanc, A., Comas, M., Balanyà, J.C., 2016. Clues for a Tortonian reconstruction of the Gibraltar Arc: Structural pattern, deformation diachronism and block rotations. Tectonophysics 683, 308–324. https://doi.org/10.1016/j.tecto.2016.05.045.

De Bruijn, H., Mein, P., Montenat, C., van der Weerd, A., 1975. Corrélations entre les gisements de rongeurs et les formations marines du Miocène terminal d'Espagne méridionale (prov. Alicante et Murcia). Proc. Koninklijke Nederlandse Akad. Wetenschappen Ser. B 78, 1–32.

De Smet, M.E.M., 1984. Wrenching in the external zone of the Betic Cordilleras, southern Spain. Tectonophysics 107, 57–79.

Durand Delga, M., Fontboté, J.M., 1980. Le cadre structural de la Méditerranée occidentale. In: BRGM (Ed.), Georogie des chaines alpines issues de la Tethys, pp. 67–85.

Esteban, M., Braga, J.C., Martín, J.M., Santisteban, C., 1996. Western Mediterranean reef complexes. In: Franseen, E.K., Esteban, M., Ward, W.C., Rouchy, J.M. (Eds.), Models for Carbonate Stratigraphy from Miocene Reef Complexes of Mediterranean Regions, Concepts in Sedimentology and Paleontology Series, vol. 5. SEPM, Tulsa, pp. 55–72.

Freudenthal, M., Mein, P., Martín-Suárez, E., 1998. Revision of late Miocene and Pliocene Cricetinae (Rodentia, Mammalia) from Spain and France. Treballs Mus. Geol. Barcel. 7, 11–93.

García-Alix, A., Minwer-Barakat, R., Martín, J.M., Martín Suárez, E., Freudenthal, M., 2008a. Biostratigraphy and sedimentary evolution of late Miocene and Pliocene continental deposits of the Granada basin (southern Spain). Lethaia 41, 431–446.

García-Alix, A., Minwer-Barakat, R., Martín-Suarez, E., Freudenthal, M., 2008b. Cricetidae and Gliridae (Rodentia, Mammalia) from the Miocene and Pliocene of southern Spain. Scr. Geol. 136, 1–37.

García-Veigas, J., Gibert, L., Cendón, D.I., Artiaga, D., Corbí, H., Soria, J.M., Lowenstein, T.K., Sanz, E., 2019. Late Miocene evaporite geochemistry of Lorca and Fortuna basins (Eastern Betics, SE Spain): evidence of restriction and continentalization. Basin Res. 00, 1–33.

Gibert, L., Orti, F., Rosell, L., 2007. Plio-Pleistocene lacustrine evaporites of the Baza Basin (Betic Chain, SE Spain). Sediment. Geol. 200, 89–116.

Gibert, L., Scott, G.R., Montoya, P., Ruiz-Sánchez, F.J., Morales, J., Luque, L., Abella, J., Lería, M., 2013. Evidence for an African-Iberian mammal dispersal during the pre-evaporitic Messinian. Geology 41, 691–694.

Gradstein, F.M., Ogg, J.G., Schmitz, M., 2012. The geologic time scale 2012, 2-volume set. Elsevier, 1176 pp.

Graham, J.W., 1949. The stability and significance of magnetism in sedimentary rocks. J. Geophys. Res. 54, 131–167.

Guerrera, F., Martín-Martín, M., 2014. Geodynamic events reconstructed in the Betic, Maghrebian, and Apennine chains (central-western Tethys). Bull. Soc. Géol. France 185, 329–341.

Haq, B., Gorini, C., Baur, J., Moneron, J., Rubino, J.L., 2020. Deep Mediterranean's Messinian evaporite giant: how much salt? Glob. Planet. Chang. 184, 103052.

Henderson, G.M., Martel, D.J., O'Nions, R.K., Shackleton, N.J., 1994. Evolution of seawater 87Sr/86Sr over the last 400 ka: the absence of glacial/interglacial cycles. Earth Planet. Sci. Lett. 128, 643–651.

Hodell, D.A., Curtis, J.H., Sierro, F.J., Raymo, M., 2001. Correlation of late Miocene to early Pliocene sequences between the Mediterranean and North Atlantic. Paleoceanography 16, 164–178.

Hoffman, K.A., 1984. A method for the display and analysis of transitional paleomagnetic data. J. Geophys. Res. 89, 6285–6292.

Kälin, D., 1999. Tribe Cricetini. In: Rössner, G.E., Heissig, K. (Eds.), The Miocene Land Mammals of Europe. Verlag Dr, Friedrich Pfeil, München, pp. 373–388.

Kayseri-Özer, M.S., 2017. Cenozoic vegetation and climate change in Anatolia—a study based on the IPR-vegetation analysis. Palaeogeogr. Palaeoclimatol. Palaeoecol. 467, 37–68.

Kirschvink, J.L., 1980. The least-squares line and plane and the analysis of palaeomagnetic data. Geophys. J. Int. 62, 699–718.

Krijgsman, W., Hilgen, F.J., Raffi, I., Sierro, F.J., Wilson, D.S., 1999. Chronology, causes and progression of the Messinian salinity crisis. Nature 400, 652–655.

Krijgsman, W., Garcés, M., Agustí, J., Raffi, I., Taberner, C., Zachariasse, W.J., 2000. The 'Tortonian salinity crisis' of the astern Betics. Earth Planet. Sci. Lett. 181, 497–511.

Krijgsman, W., Fortuin, A.R., Hilgen, F.J., Sierro, F.J., 2001. Astrochronology for the Messinian Sorbas basin (SE Spain) and orbital (precessional) forcing for evaporite cyclicity. Sediment. Geol. 140, 43–60.

Krijgsman, W., Capella, W., Simon, D., Hilgen, F.J., Kouwenhoven, T.J., Meijer, P.T., Sierro, F.J., Tulbure, M.A., van der Berg, B.C.J., van der Schee, M., Flecker, R., 2018. The Gibraltar Corridor: Watergate of the Messinian Salinity Crisis. Mar. Geol. 403, 238–246.

Lindke, J., Ziegenbalg, S.B., Brunner, B., Rouchy, J.M., Pierre, C., Peckmann, J., 2011. Authigenesis of native Sulphur and dolomite in a lacustrine evaporitic setting (Hellín basin, late Miocene, SE Spain). Geol. Mag. 148, 655–669.

Lirer, F., Foresi, L.M., Iaccarino, S.M., Salvatorini, G., Turco, E., Cosentino, C., Sierro, F. J., Carusso, A., 2019. Mediterranean Neogene planktonic foraminífer biozonation and biochronology. Earth Sci. Rev. 196, 102869.

Lonergan, L., White, N., 1997. Origin of the Betic-Rif Mountain Belt. Tectonophysics 16, 504–522.

Mansino, S., Fierro, I., Ruiz-Sánchez, F.J., Montoya, P., 2013. The fossil rodent faunas of the localities Alcoy 2C and 2D (Alcoy Basin, Spain). Implications for dating the classical locality of 2 Alcoy-Mina. J. Iber. Geol. 39, 261–284.

Mansino, S., Fierro, I., Montoya, P., Ruiz-Sánchez, F.J., 2015. Micromammal faunas from the Mio-Pliocene boundary in the Alcoy Basin (SE Spain): biostratigraphical and palaeoecological inferences. Bull. Geosci. 90, 555–576.

Mansino, S., Fierro, I., Tosal, A., Montoya, P., Ruiz-Sánchez, F.J., 2017a. Micromammal biostratigraphy of the Alcoy Basin (Eastern Spain): remarks on the Pliocene record of the Iberian Peninsula. Geol. Acta 15, 121–134.

Mansino, S., Crespo, V., Montoya, P., Ruiz-Sánchez, F.J., 2017b. Muridae from the late Miocene site of Venta del Moro (Eastern Spain). Hist. Biol. 29, 677–691.

McArthur, J.M., Howarth, R.J., Shields, G.A., 2012. Chapter 7: Strontium isotope stratigraphy. In: Gradstein, F.M., Ogg, J.G., Schmitz, M. (Eds.), The Geologic Time Scale 2012, Vol. 1. Elsevier, pp. 127–144.

Manzi, V., Gennari, R., Hilgen, F., Krijgsman, W., Lugli, S., Roveri, M., Sierro, F.J., 2013. Age refinement of the Messinian salinity crisis onset in the Mediterranean. Terra Nova 25, 315–322.

Meijers, M.J.M., Peynircioglu, A.A., Cosca, M.A., Brocard, G.Y., Whitney, D.L., Langereis, C.G., Mulch, A., 2018. Climate stability in Central Anatolia during the Messinian Salinity Crisis. Palaeogeogr. Palaeoclimatol. Palaeoecol. 498, 53–67.

Mein, P., Moissenet, E., Adrover, R., 1990. Biostratigraphie du Néogène Supérieur du basin de Teruel. Paleontol.Evol. 23, 121–139.

Morales, J., Peláez-Campomanes, P., Abella, J., Montoya, P., Ruiz-Sánchez, F.J., Gibert, L., Scott, G., Cantalapiedra, J.L., Sanisidro, O., 2013. The Ventian mammal age (Latest Miocene): present state. Span. J. Palaeontol. 28, 149–160.

Ortí, F., Rosell, L., 2000. Evaporative systems and diagenetic patterns in the Calatayud Basin (Miocene, Central Spain). Sedimentology 47, 665–685.
Ortí, F., Rosell, L., Anadón, P., 2003. Deep to shallow lacustrine evaporites in the Libros Gypsum (southern Teruel Basin, Miocene, NE Spain): an occurrence of pelletal gypsum rhytmites. Sedimentology 50, 361–386.
Ortí, F., Rosell, L., Playà, E., García-Veigas, J., 2010. Large gypsum nodules in the Paleogene and Neogene evaporites of Spain: distribution and palaeogeographic significance. Geol. Q. 54, 411–422.
Ortí, F., Pérez-López, A., García-Veigas, J., Rosell, L., Cendón, D.I., Pérez-Valera, F., 2014. Sulfate isotope compositions (δ34S, δ18O) and strontium isotopic ratios (87Sr /86Sr) of Triassic evaporites in the Betic Cordillera (SE Spain). Rev. Soc. Geol. Esp. 27, 79–90.
Ortí, F., Pérez-López, A., Pérez-Valera, F., Benedicto, C., 2022. Isotope composition (δ34S, δ18O) of the Middle Triassic-early Jurassic sulfates in eastern Iberia. Sediment. Geol. 431, 106104.
Paquet, J., Kampschuur, W., Baena, J., Velando, F., García-Monzón, G., Rondeel, H.E., 1974. Mapa geológico y memoria de la hoja n° 932 (Coy). In: Mapa Geológico de España E. 1:50000. Segunda Serie (MAGNA), Primera edición. IGME.
Pineda, V., Gibert, L., Soria, J.M., Carrazana, A., Ibáñez-Insa, J., Sánchez-Román, M., 2021. Interevaporitic deposits of Las Minas Gypsum Unit: a record of late Tortonian marine incursions and dolomite precipitation in Las Minas Basin (eastern Betic Cordillera, SE Spain). Palaeogeogr. Palaeoclimatol. Palaeoecol. 564, 110171.
Piñero, P., Agustí, J., Oms, O., Fierro, I., Montoya, P., Mansino, S., Ruiz-Sánchez, F., Alba, D.M., Alberdi, M.T., Blain, H.A., 2017. Early Pliocene continental vertebrate fauna at Puerto de la Cadena (SE Spain) and its bearing on the marine-continental correlation of the late Neogene of Eastern Betics. Palaeogeogr. Palaeoclimatol. Palaeoecol. 479, 102–114.
Piñero, P., Agustí, J., 2019. The rodent succession in the Sifón de Librilla section (Fortuna Basin, SE Spain): implications for the Mio-Pliocene boundary in the Mediterranean terrestrial record. Hist. Biol. 31, 279–321.
Rodriguez-Aranda, J.P., Calvo, J.P., 1998. Trace fossils and rhizoliths as a tool for sedimentological and palaeoenvironmental analysis of ancient continental evaporite succesions. Palaeogeogr. Palaeoclimatol. Palaeoecol. 140, 383–399.
Rouchy, J.M., 1982. La Genèse des évaporites Messiniennes de Méditerrannée. In: Mémoires du Muséum National d'Historie Naturelle, 38.
Rouchy, J.M., Carusso, A., 2006. The Messinian salinity crisis in the Mediterranean basin: a reassessment of the data and an integrated scenario. Sediment. Geol. 188–189, 35–67.
Roveri, M., Gennari, R., Lugu, S., Manzi, M., 2009. The Terminal Carbonate complex: the record of sea-level changes during the Messinian salinity crisis. GeoActa 8, 63–77.
Ruiz-Sánchez, F.J., Freudenthal, M., Mansino, S., Crespo-Roures, V.D., Montoya, P., 2014. Apocricetus barrierei (Rodentia, Mammalia) from La Bullana 2B and La Bullana 3 (Cabriel Basin, Valencia, Spain). Revision of the late Miocene-early Pliocene forms of the genus Apocricetus. Paläontol. Z. 88, 85–98.
Ryan, W.B.F., 1973. Geodynamic implications of the Messinian crisis of salinity. In: Drooger, C.W. (Ed.), Messinian Events in the Mediterranean. North-Holland Publ, Co, Amsterdam, Netherlands, pp. 26–38.
Salvany, J.M., Ortí, F., 1990. Parada 12: Campo Coy (Mioceno Superior). In: Ortí, F., Salvany, J.M. (Eds.), Formaciones Evaporíticas de la Cuenca del Ebro Y Cadenas Periféricas, Y de la Zona de Levante. Universitat de Barcelona-ENRESA, Barcelona, pp. 294–297.
Sánchez-Román, M., Vasconcelos, C., Schmidt, T., Dittrich, M., McKenzie, J.A., Zenobi, R., Rivadeneyra, M.A., 2008. Aerobic microbial dolomite at the nanometer scale: Implications for the geologic record. Geology 36, 879–882.
Sánchez-Román, M., Vasconcelos, C., Warthmann, R., Rivadeneyra, M.A., McKenzie, J. A., Mckenzie, J.A., 2009. Microbial dolomite precipitation under aerobic conditions: results from Brejo do Espinho lagoon (Brazil) and culture experiments. In: Swart, P. K., Eberli, G.P., Jarvis, I., Stevens, T. (Eds.), Perspectives in Carbonate Geology: A Tribute to the Career of Robert Nathan Ginsburg. Sedimentology, IAS Special Publication No. 40, pp. 167–178.
Sánchez-Román, M., Romanek, C.S., Fernández-Remolar, D.C., Sánchez-Navas, A., McKencie, J.A., Pibernat, R.A., Vasconcelos, C., 2011. Aerobic biomineralization of Mg-rich carbonates: Implications for natural environments. Chem. Geol. 281, 143–150.
Sanz de Galdeano, C., 1990. Geologic evolution of the Betic Cordilleras in Western Mediterranean, Miocene to the present. Tectonophysics 172, 107–119.
Soria, J.M., Fernández, J., Viseras, C., 1999. Late Miocene stratigraphy and paleogeographic evolution of the intramontane Guadix Basin (Central Betic Cordillera, Spain): implications for an Atlantic-Mediterranean connection. Palaeogeogr. Palaeoclimatol. Palaeoecol. 151, 255–266.
Soria, J.M., Caracuel, J.E., Corbí, H., Dinarès-Turell, J., Lancis, C., Ten Manclús, J.E., Viseras, C., Yébenes, A., 2008. The Messinian–early Pliocene stratigraphic record in the southern Bajo Segura Basin (Betic Cordillera, Spain): Implications for the Mediterranean salinity crisis. Sediment. Geol. 203, 267–288.
Talbot, M.R., 1990. A review of the palaeohydrological interpretation of carbon and oxygen isotopic ratios in primary lacustrine carbonates. Chem. Geol. 80, 261–279.
Tent-Manclús, J.E., Soria, J.M., Estévez, A., Lancis, C., Caracuel, J.E., Dinarès-Turell, J., Yébenes, A., 2008. The Tortonian salinity crisis in the Fortuna Basin (southeastern Spain): Stratigraphic record, tectonic scenario and chronostratigraphy. Compt. Rendus Geosci. 340, 474–481.
Uchman, A., Nemec, W., Ilgar, A., Messina, C., 2007. Lacustrine trace fossils and environmental conditions in the early Miocene Ermenek Basin, southern Turkey. Ann. Soc. Geol. Pol. 77, 123–139.
Van Couvering, J.A., Castradori, D., Cita, M.B., Hilgen, F.J., Rio, D., 2000. The base of the Zanclean Stage and of the Pliocene Series. Episodes 23, 179–187.
Vasiliev, I., Mezger, E.M., Lugli, S., Reichart, G.J., Manzi, V., Roveri, M., 2017. How dry was the Mediterranean during the Messinian salinity crisis? Palaeogeogr. Palaeoclimatol. Palaeoecol. 471, 120–133.
Warren, J.K., 2006. Chapter 1: Interpreting evaporite texture. In: Warren, J.K. (Ed.), Evaporites, Sediments and Hydrocarbons. Springer Science + Business Media, Berlin, pp. 1–57.